chemosensors

MDPI

Review

Recent Progress in MXenes-Based Materials for Gas Sensors and Photodetectors

Praveen Kumar [1,†], Waseem Raza [2,3,†], Sanjeevamuthu Suganthi [4,†], Mohd Quasim Khan [5], Khursheed Ahmad [4,*] and Tae Hwan Oh [4,*]

[1] Department of Chemistry, Indian Institute of Technology Indore, Simrol, Indore 453552, India
[2] Department of Materials Science and Engineering, WW4-LKO, University of Erlangen-Nuremberg, Martensstrasse 7, 91058 Erlangen, Germany
[3] Department of Chemistry and Biochemistry, Facultad de Farmacia, Universidad CEU San Pablo, Urbanización Montepríncipe, Boadilla del Monte, 28668 Madrid, Spain
[4] School of Chemical Engineering, Yeungnam University, Gyeongsan 38541, Republic of Korea
[5] Department of Chemistry, M.M.D.C, Moradabad, M.J.P. Rohilkhand University, Bareilly 244001, India
* Correspondence: khursheed@yu.ac.kr (K.A.); taehwanoh@ynu.ac.kr (T.H.O.)
† These authors contributed equally to this work.

Abstract: Recently, a new class of two-dimensional (2D) materials known as MXenes, such as $Ti_3C_2T_x$, have received significant attention due to their exceptional structural and physiochemical properties. MXenes are widely used in a variety of applications, including sensors, due to their excellent charge transport, high catalytic, and conducive properties, making them superior materials for sensing applications. Sensing technology has attracted significant interest from the scientific community due to its wide range of applications. In particular, gas sensing technology is essential in today's world due to its vital role in detecting various gases. Gas sensors have an essential role in real-time environmental monitoring health assessment, and the demand for air quality monitoring is driving the gas sensor market forward. Similarly, optical sensors are a related technology that can rapidly detect toxic substances and biomaterials using optical absorption spectroscopy. MXenes are highly desirable for gas and optical sensing applications due to their abundant active sites, metallic conductivity, optical properties, customizable surface chemistry, and exceptional stability. In this review article, we compile recent advancements in the development of gas sensors and optical sensors using MXenes and their composite materials. This review article would be beneficial for researchers working on the development of MXenes-based gas sensors and optical sensors.

Keywords: MXene; gas sensors; optical sensors; two-dimensional material

check for updates

Citation: Kumar, P.; Raza, W.; Suganthi, S.; Khan, M.Q.; Ahmad, K.; Oh, T.H. Recent Progress in MXenes-Based Materials for Gas Sensors and Photodetectors. *Chemosensors* **2024**, *12*, 147. https://doi.org/10.3390/chemosensors12080147

Received: 29 May 2024
Revised: 9 July 2024
Accepted: 23 July 2024
Published: 1 August 2024

Copyright: © 2024 by the authors. Licensee MDPI, Basel, Switzerland. This article is an open access article distributed under the terms and conditions of the Creative Commons Attribution (CC BY) license (https://creativecommons.org/licenses/by/4.0/).

1. Introduction

Recently, the enormous utilization of two-dimensional (2D) materials has drawn significant attention to various applications from the scientific community [1–4]. The optoelectronic applications such as energy storage, generation, sensing, catalysis, and optoelectronics leverage 2D materials due to their fascinating physical and optical properties [5–12]. Since the discovery of graphene, there has been rapid growth in the synthesis and utilization of 2D materials, including boron nitride, perovskite materials, metal halides, and transition metal halides [13–18]. Their structural flexibility and wide range of compositions have attracted considerable attention, leading to their use in diverse applications [19–23]. In 2011, a new type of 2D material was discovered by Gogotsi and his research team, which known as MXene [24]. MXenes are generally synthesized via a unique etching synthesis procedure [25]. The synthesis of MXenes involves etching layers from the bulk MAX phase using hydrofluoride (HF) as an etchant. Surface functionalization, achieved through exfoliation and etching during MXene synthesis, introduces hydrophilicity, with further modifications possible through calcination or alkalization for specific applications [26]. The

MAX phase consists of early d-block transition metals (M), group 13–15 elements (A), and carbon or nitrogen (X) [27]. It features a closely packed multi-layered structure ($M_{n+1}AX_n$ layers, with n ranging from 1 to 4) of ternary carbides and nitrides [28]. Although the M-A bonds are strong, the presence of the covalent, metallic, and ionic characters of the M-X bonds facilitate the chemical etching of the A layer during the synthesis of the MXene [24]. The wide variety of stoichiometric compositions of MAX phases allows for the formation of numerous MXenes, offering significant diversity and thermodynamic stability with excellent electrical conductivity [29]. These properties make MXenes promising for extensive research and various applications due to their outstanding electrical conductivity, excellent mechanical stability, large specific surface areas, and good hydrophilicity [30].

In the current era of information sensing, the detection, and analysis of information play vital roles across various fields [31]. Conventional sensors are used to detect chemical reactions, biological interactions, and physical variables [32]. Sensors are the new generation technologies which can significantly detect variations in targeted detection, then convert signals into optical, electrical, or thermal outputs for transmission, processing, and storage [33–35]. It is expected that an ideal sensor should be highly sensitive and highly selective, with a low detection limit and fast response time [36–38]. The demand for high sensitivity and fast response has driven the scientific community to explore newly synthesized materials for sensor fabrication [39]. MXenes have emerged as suitable candidates due to their large specific surface area and high electrical conductivity [40], which may be attributed to the presence of metal-like properties in the MXene [41], surface functional groups that provide good hydrophilicity [42], and a stable structure that resists oxidation under harsh conditions [43]. MXenes are employed in various optical sensors, including electrochemiluminescence (ECL), surface plasmonic, SERS, and fluorescent sensors. Modifying MXenes with other nanomaterials and functionalization can enhance their properties and expand their applications [44]. Transforming MXenes into nanosheets or quantum dots is particularly advantageous for SERS substrates, fluorescence quenchers, and photoluminescent materials [45,46]. The favorable energy levels of MXene nanosheets, due to their wide absorption, provide an excellent platform for the fabrication of photo–thermal, photo–electrochemical, and optical sensors [47]. MXenes have also shown exceptional promise for optical sensors due to their remarkable optical properties, such as photoluminescence, transmittance, surface-enhanced Raman scattering (SERS), and absorption, motivating their use in sensor design and fabrication [48–50]. Based on sensing signals, the most efficient and reasonable MXene-based sensors can be categorized into optical and electrical sensors.

The next generation technological progress in recent years has resulted in the proliferation of smart devices across many aspects of our lives [51]. From smartphones to wearable fitness trackers, the need for innovative and efficient sensing technologies is at an all-time high [52]. Especially in the field of gas sensing, there has been substantial advancement due to the necessity of monitoring air quality, detecting hazardous gases and industrial emissions for healthcare and smart home applications [53,54]. Smart gas sensors mark a significant departure from traditional gas detection techniques [54]. Although conventional gas sensors have been in use for many years, they frequently face challenges regarding sensitivity, cost-effectiveness, data processing abilities, and power efficiency [55]. On the other hand, smart gas sensors guide us towards state-of-the-art technologies and advanced materials, offering numerous benefits and making them indispensable across various applications [56].

Optical sensors have emerged as powerful tools in various fields, offering precise and sensitive detection capabilities [57]. Optical sensors have gained attention, particularly in biosensor fabrication, due to their high selectivity and sensitivity, quick response time, cost-effectiveness, and reproducibility [58]. The ability of the optical sensors to convert changes in light properties into measurable signals has enabled their use in diverse applications such as environmental monitoring, biomedical diagnostics, and industrial process control [59,60]. In the past few years, MXenes either alone or its hybrid composites, have been extensively used for the detection of various biological and chemical analytes using gas and optical

sensing technologies. In the present review article, we have summarized the reported articles on the fabrication of gas and optical sensors using MXenes and their composites. We believe that the present review article would be useful for the research scholars and scientists working on the design and fabrication of MXene-based gas and optical sensors.

2. MXene Synthesis

Synthesizing MXene follows a process akin to other 2D materials, involving the exfoliation of layers from raw materials. Initially, researchers attempted mechanical exfoliation on MAX phase precursors, akin to the process used for graphite. However, due to the robust M-A bonds inherent in MAX, obtaining pure MXene proved challenging. Consequently, researchers explored suitable etching methods to remove the "A" atom layer from MAX, employing etchants such as concentrated HF or HF containing hydrochloric acid–lithium fluoride salts (LiF/HCl) [61]. Ultrasonic treatment facilitated the etching process for MXene synthesis, with the resultant crude product subjected to washing to eliminate residual substances, followed by vacuum drying. To obtain MXene sheets, further detachment or delamination of the multi-layered MXene was achieved through intercalation, employing organic molecules, cations, or organic bases via ultrasonication and centrifugation processes [62,63]. Intercalation is a crucial step for producing free-standing MXene sheets, yielding an aqueous colloidal solution of MXene. This method, also known as the wet etching method, stands as a well-established top-down approach for MXene synthesis.

The initial synthesis of the first MXene, Ti_3C_2, involved the removal of the Al layer from the MAX Phase (Ti_3AlC_2) through etching with 50% HF acid, as in the reaction:

$$Ti_3AlC_2 + HF \text{ ---------- } AlF_3 + Ti_3C_2 + 3/2H_2$$

This process exploited the weaker Ti-Al bonds compared to the Ti-C bonds, facilitating the detachment of the Al layer and leaving functional groups attached to the MXene surface [62]. The resulting $M_{n+1}X_nT_x$ MXene exhibited a multilayered structure with strong bonding between layers, attributed to van der Waals forces or H-bonding. The duration of HF etching and the temperature varied, influencing the outcome from hours to days and from room temperature to 50 °C [64,65]. Ti_3C_2, like other MXenes, demonstrated dispersibility in both organic and aqueous solutions, such as propylene carbonate, ethanol, and dimethylformamide (DMF), enabling its incorporation with polymers and nanomaterials through solvent exchange, mixing, or self-assembly [66]. The use of concentrated HF acid as an etchant posed environmental and health risks due to its highly corrosive nature. Consequently, safer alternatives have been developed, such as the HF-forming etchant method, which utilizes hydrolysis of bifluoride salts to produce HF in situ. This method offers advantages over raw HF, including safety, high yield, flexibility, and shorter sonication time [67].

Notably, the combination of LiF–HCl has been employed in synthesizing high-quality MXene sheets of Ti_3C_2 and Mo_2C [68], where Li^+ ions in the etchant solution facilitate concurrent etching and intercalation [69]. Factors like reaction conditions, composition, etching solution, time, and MAX phase particle size affect MXene yield and quality, with prolonged etching potentially causing structural defects, especially in M_4AX_3 MAX phases, which require harsher etching conditions than other MAX phases like M_3AX_2 [70].

Surface functionalities such as –O, –OH, and –F depend on the synthesis method, with –F and –O functionalities predominating in MXenes produced via the HF etching and LiF/HCl processes, respectively [71]. Beyond the top-down approach, a bottom-up approach involving techniques like plasma-enhanced pulsed laser deposition (PEPLD), template methods, and chemical vapor deposition (CVD) has been recommended for high-quality MXene synthesis. For instance, CVD has been utilized to synthesize ultrathin crystals of transition metal carbides/nitrides (TMC/TMN) [72], while the template method using 2D transition metal oxides facilitated the synthesis of MXenes by ammoniating or carbonizing [73]. Also, this template method was used in development of nanosheets

of MoN and other nitrides [74]. PEPLD, employing both ionized and non-ionized CH_4 plasma, has been successful in synthesizing high-quality ultrathin Mo_2C crystals [75].

3. MXenes in Gas Sensors

Gas sensors are attracting significant global attention for their crucial role in accurately detecting various toxic gases, which is essential for monitoring environmental health. Gas sensors are used in various fields such as medical diagnostics, domestic and public security, environmental monitoring, industrial production, and food safety [76,77]. The fundamental function of gas sensors is to convert the composition and concentration of gas into electrical signals, facilitating their detection. Extensive efforts have been made and reported in the literature focusing on the detection of toxic and explosive gases for environmental monitoring. For this, various approaches have been investigated, such as conductive polymers, metal oxide semiconductors (MOS), carbon-based materials, and two-dimensional (2D) materials [78,79]. These sensor materials offer numerous advantages such as low detection limits, rapid response and recovery times, high sensitivity, excellent stability, a simple fabrication process, and low cost. Among these sensor materials, MOS are the most extensively explored materials for gas sensing applications. However, MOS requires external stimuli such as high temperatures for adsorption and desorption of gas molecules or ultraviolet light to alter the conductive properties of sensors. This dependency can lead to increasing power consumption, higher costs, and a greater risk of ignition for flammable gases. Hence, there is a significant focus on conducting extensive research to develop advanced gas sensors with low detection limits that can operate effectively at room temperature.

MXene belongs to a novel class of 2D materials and has emerged as a promising candidate in gas sensing applications [80,81]. When compared with other 2D materials such as graphene and transition metal dichalcogenides (TMDs), MXene is attracting greater attention in the field of gas sensing [82]. Due to its facile synthesis methods and unique properties, MXene has become a central point for scientists, leading to a significant number of articles in the literature as depicted in Figure 1 [63].

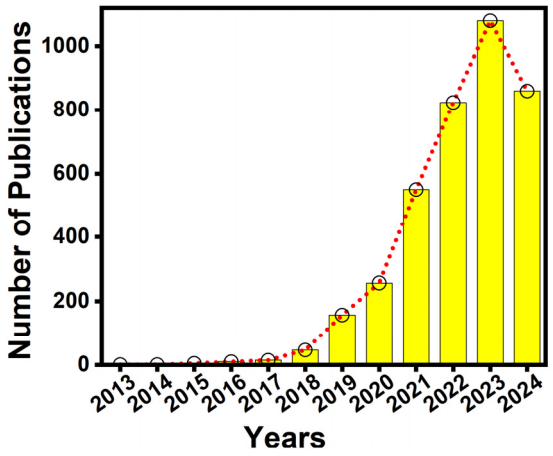

Figure 1. The annual number of publications on MXene in gas sensing and other fields.

Furthermore, the rapid growth of MXene in sensing has surpassed graphene and TMDs. This has positioned MXene as a promising material for gas sensing and it has gained increasing attention due to its remarkable electrical conductivity, hydrophilic surface, large specific surface area, abundant surface functional groups, excellent stretchability, and biocompatibility [83–85]. These distinctive characteristics that make MXene well-suited for gas sensing applications may be attributed to the presence of M and X sites within its structure. These sites offer tunable surface functionalities, which promote a high adsorption energy of gases, enhancing their sensitivity and selectivity in gas sensing [86]. In addition to its surface properties, MXene exhibits other versatile functionalities such

as robust mechanical strength, exceptional stability, good volumetric capacity, significant zeta potential, and rapid ionic transport (Figure 2). These collective features improve its selectivity for various toxic gases, even in very low signal to noise. These unique properties of MXene have inspired scientists to concentrate on MXene-based materials for gas sensing applications rather than other 2D materials [87].

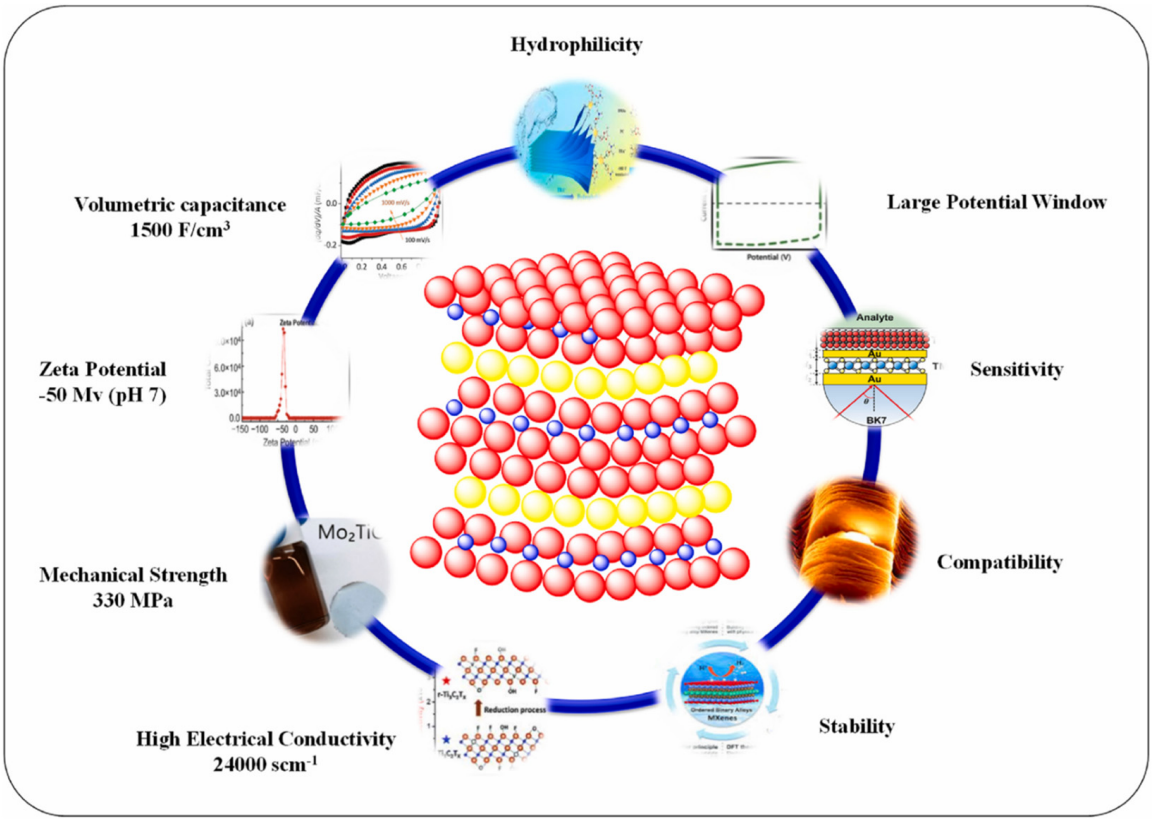

Figure 2. A schematic illustration of MXene properties typically shows its surface functional groups, high electrical conductivity, mechanical flexibility, and other notable features [88].

MXene has been demonstrated to be an extremely sensitive platform for selectively detecting a broad range of gases. Moreover, MXene exhibits a rapid gas sensing response even at room temperature by quickly absorbing gas molecules from the environment. Gas sensors based on MXene have exhibited remarkable gas-sensing applications. Notable examples include $Ti_3C_2T_X$, $Ti_3C_2T_X$/ZnO, and $Ti_3C_2T_X$/$Mo_2T_xCo_3O_4$@PEI [89–93].

3.1. Pristine MXene-Based Gas Sensor

Numerous research studies have been published based on pristine Ti_3C_2Tx sensors, demonstrating superior selectivity and sensitivity compared to traditional room temperature gas sensors. Yu and their co-workers explored the gas sensing capabilities of one of the thinnest (Ti_2CO_2) layers of the MXene family towards ammonia sensing [94]. They utilized the non-equilibrium Green's function method to calculate the current–voltage (I–V) relation for NH_3, indicating a significant change in the I–V curve before and after NH_3 absorption on TiC_2CO_2 due to the distinct transport properties of NH_3. To assess the sensitivity of the prepared sensor, they investigated the adsorption of different gases such as NH_3, H_2, CO, CO_2, CH_4, N_2, NO_2, and O_2 using first principles simulations. It can be seen from Figure 3 that the chemisorption of NH_3 on the Ti_2CO_2 sensor is notably high as compared to other analytes, possibly due to biaxial strain, indicating a weak interaction with other gases. This suggested that detecting ammonia using biaxial strain on a monolayer of Ti_2CO_2 is preferable over other gases. Moreover, the nitrogen atom of ammonia demonstrates a strong binding interaction with the titanium of Ti_2CO_2 as compared to other analytes.

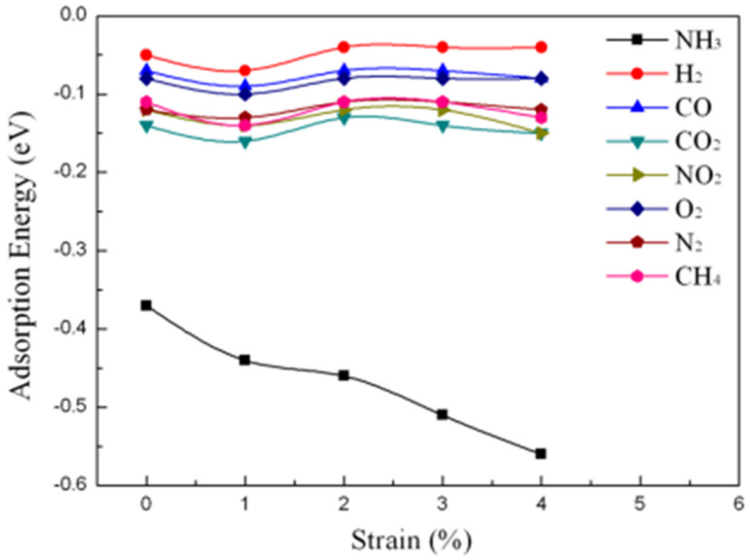

Figure 3. Adsorption behavior of different analytes on the surface of the Ti_2CO_2 sensor as a function of applied biaxial strains [94].

This strong binding is attributed to the positioning of the N atom of NH_3 exactly above the Ti atom, resulting in a high binding energy, as shown in Figure 4a,b [94]. They found that the conductivity of the Ti_2CO_2 sensor was found to be increased upon adsorption of ammonia under the strain, indicating a high sensitivity towards ammonia as compared to other analytes under strain. The promising adsorption or desorption of ammonia on the Ti_2CO_2 sensor is attributed to its high adsorption energy (0.37 eV) and high charge transfer (0.174 electrons). Therefore, the absorption of ammonia is reversible, suggesting that the Ti_2CO_2 sensor is well-suited for ammonia sensing [94].

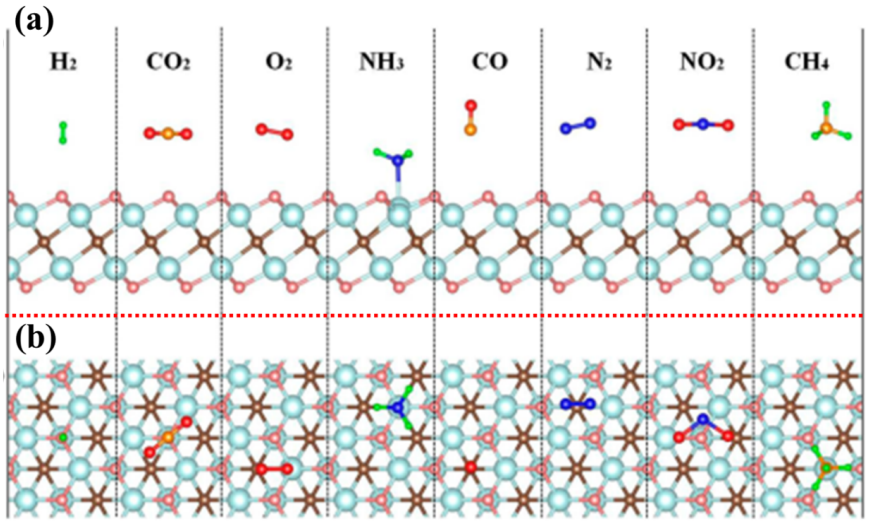

Figure 4. Schematic illustration of the adsorption of different gas molecules on the monolayer of the Ti_2CO_2 sensor surface: (**a**) side view and (**b**) top view [94].

In addition to the work on the Ti_2CO_2 monolayer, a similar study on ammonia sensing using the Zr_2CO_2 MXene have been reported in the literature [95]. This study demonstrated a systematic investigation of the adsorption/desorption behavior of ammonia on an O-functionalized Zr_2CO_2 MXene with both negative and neutral charges, using first principles simulations. The result indicates a nearly similar adsorption behavior of ammonia on the Zr_2CO_2 MXene, like the Ti_2CO_2 MXene. They demonstrated that the adsorption behavior of ammonia on the Zr_2CO_2 MXene monolayer is highly favorable as compared to other

gases, with significant charge transfer. This favorable adsorption is attributed to the large adsorption energy (0.81 eV) and Mulliken charge transfer (0.188). Moreover, ammonia molecules can be efficiently desorbed from the monolayer of the Zr_2CO_2 MXene by injecting electrons from ammonia to the Zr_2CO_2 MXene [95].

They observed that the adsorption behavior of other gases (such as H_2, CH_4, CO, CO_2, N_2, and O_2) on the Zr_2CO_2 sensor surface differs significantly from that of ammonia. This difference arises from variations in adsorption energies and Mulliken charge transfer between ammonia and other gas molecules when interacting with the Zr_2CO_2 sensor surface, as depicted in Figure 5 [95]. Since the charge transfer between gases and sensors is crucial for the gas sensing performance, a Hirshfeld charge analysis was carried out to further validate the results. As illustrated in Figure 5, the Hirshfeld charge transfer between ammonia and the Zr_2CO_2 sensor is found to be 0.223 e, which is larger than the other gases. These results are consistent with the Mulliken charge analysis findings. Hence, O-functionalized Zr_2CO_2 MXenes emerge as a promising candidate for ammonia sensing with high selectivity [95].

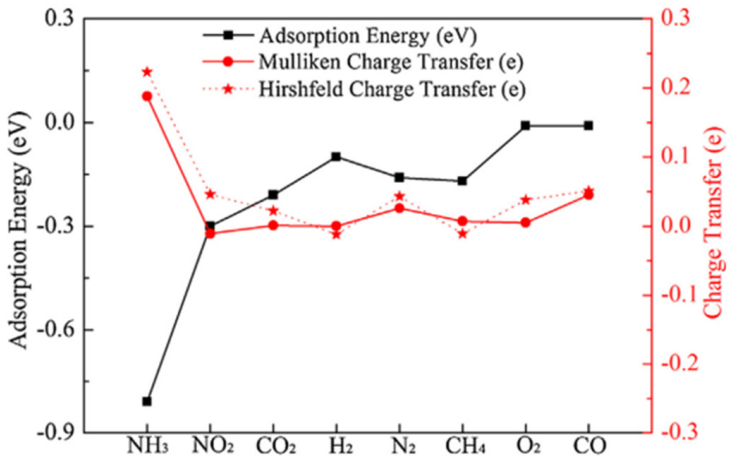

Figure 5. Adsorption behavior and Mulliken/Hirshfeld charge transfer for different gas molecules on the Zr_2CO_2 sensor surface [95].

Mai et al. investigated the sensing behavior of SO_2 on an O-functionalized M_2CO_2 (M = Sc, Hf, Zr, and Ti) monolayer due to the highly toxic nature of SO_2, which can pose different human health risks [96]. The sensing behavior of SO_2 on the Sc_2CO_2 sensor monolayer was qualitatively investigated using first principles calculations. They used two-probe models to estimate the relationship between I and V before and after the SO_2 adsorption, as shown in Figure 6a. The I–V graph exhibited a significant increase in the current after adsorption of SO_2 on a sensor, as shown in Figure 6b. These findings suggest that the Sc_2CO_2 monolayer is a promising sensor for SO_2 sensing.

In another study, Yang et al. also explored the gas sensing capabilities of the Sc_2CO_2 monolayer for detecting carbon monoxide (CO) and nitrogen oxide (NO) [97]. They observed that the Sc_2CO_2 monolayer exhibited good sensitivity to the NO molecule due to a chemical interaction and a significant charge transfer of 0.303 e, which was further increased by applying external strain. Conversely, the sensitivity towards CO was found to be increased after Mn doping into Sc_2CO_2, attributed to the strong adsorption energy (−0.85 eV) [97]. In 2017, Lee et al. developed a flexible room temperature gas sensor by fabricating a $Ti_3C_2T_X$ nanosheet on a polyimide substrate using a simple drop cast method [98]. This sensor demonstrated effective detection capabilities for various polar gases such as methanol, ethanol, acetone, and ammonia even at concentrations as low as 100 ppm at room temperature. The fabricated sensor exhibited p-type sensing behavior. The fabricated sensor exhibited the dynamic gas response of $Ti_3C_2T_X$ and was found to be 21, 14.3, 11.5, and 7.5% for ammonia, methanol, ethanol, and acetone, respectively, as shown in Figure 7 [98].

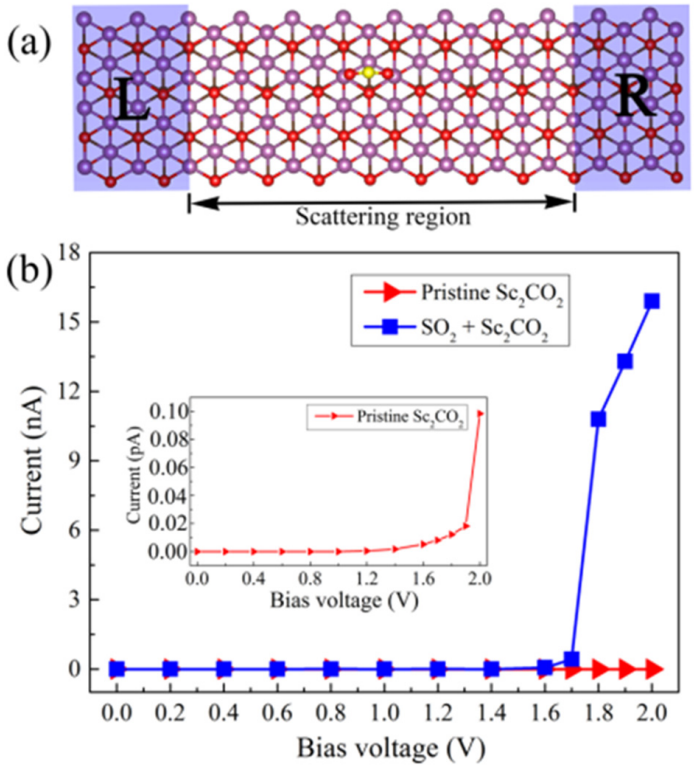

Figure 6. (**a**) Illustration of two-probe model of Sc_2CO_2 monolayer for SO_2 sensing and (**b**) I–V relation of pristine and SO_2-adsorbed Sc_2CO_2 monolayer sensor. The inset in (**b**) indicates the I–V relation of the pristine Sc_2CO_2 monolayer sensor without SO_2 gas [96].

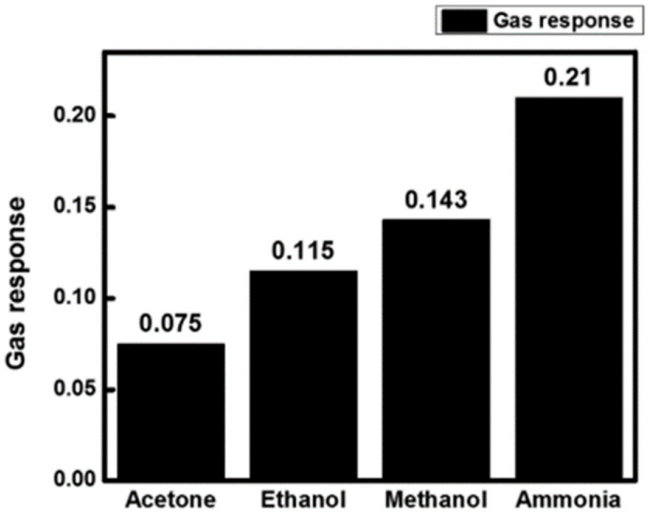

Figure 7. The calculated gas response of different polar gases towards the $Ti_3C_2T_X$ sensor [98].

In a p-type sensor, most carriers are holes, which shows a reduction due to the transfer of electrons from the gases to the predominating surface terminal groups, resulting in an increase in resistance. The fabricated sensor showed the lowest response to acetone (7.5%), whereas it showed the highest response to ammonia (21%), with a theoretical limit of detection of 9.27 ppm [98]. It can be seen from Figure 8, that the resistance of the $Ti_3C_2T_X$ sensor improved upon the introduction of gaseous molecules and decreased when the gases were removed [98].

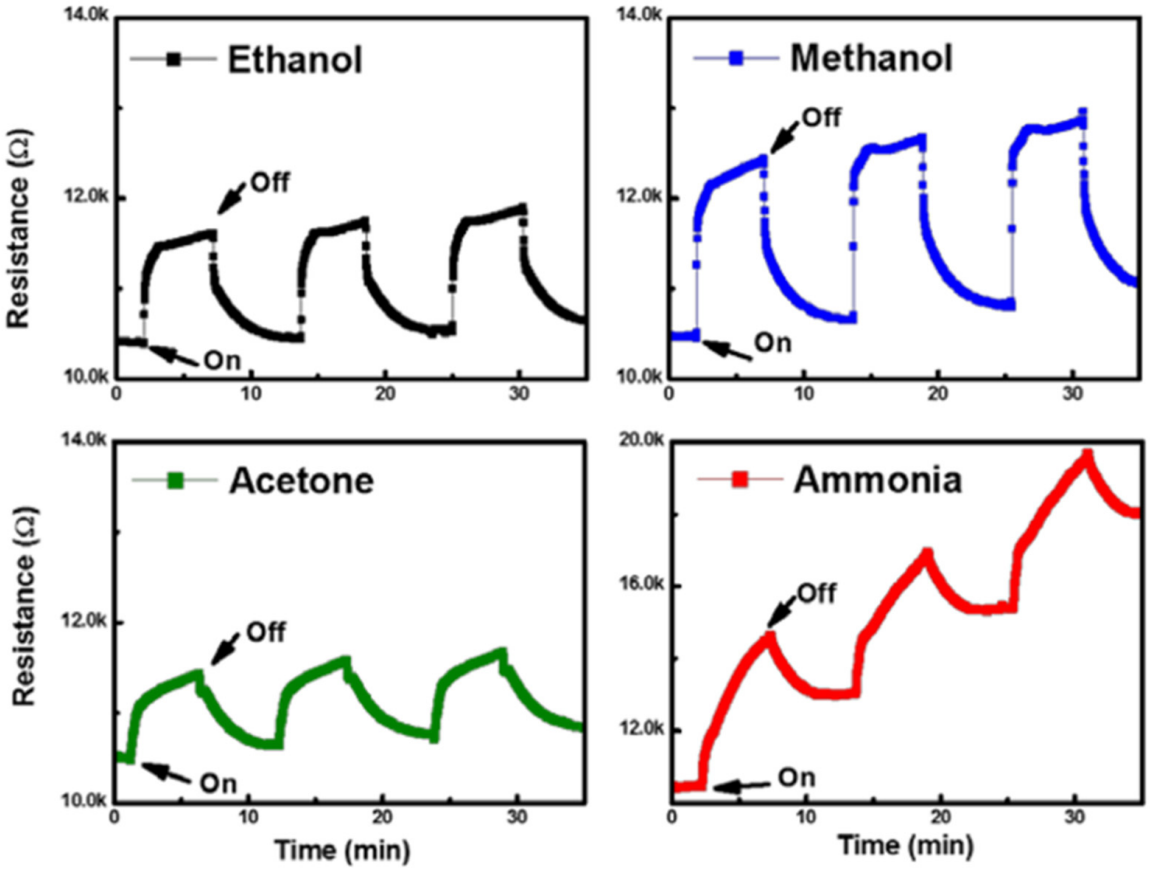

Figure 8. The gas sensing response of the $Ti_3C_2T_X$ sensor towards 100 ppm ethanol, methanol, acetone, and ammonia at ambient environmental conditions [98].

A plausible sensing mechanism of the fabricated sensor was proposed focusing on the charge interaction between gaseous molecules and the surface functional groups (–O, –OH) of the $Ti_3C_2T_X$ sensor (Figure 9a). For example, the mechanism elucidating ammonia sensing over the $Ti_3C_2T_X$ sensor is schematically depicted in Figure 9b [98]. The $Ti_3C_2T_X$ sensor exhibited an alteration in the electrical response upon the efficient adsorption or desorption of the gaseous molecule on its surface. Specifically, when a gas molecule like ammonia is absorbed into the terminal groups such as $–O^-$ and $–OH^-$ of the $Ti_3C_2T_X$ sensor, electrons are generated through Equations (1) and (2). These electrons then combined with the holes present in the $Ti_3C_2T_X$ sensor, indicating electron–hole recombination and subsequently resulting in an increase in the resistance [98].

$$2NH_3 + 3O^- = N_2 + 3H_2O + 3e^- \quad (1)$$

$$NH_3 + OH^- = NH_2 + H_2O + e^- \quad (2)$$

Following the initial demonstration of the $Ti_3C_2T_X$ gas sensor, Kim and co-workers have advanced their research by developing an ultrahigh chemo resistive gas sensor based on $Ti_3C_2T_X$, aiming for the precise detection of volatile organic compounds (VOCs) [99]. Their experiment design involved fabricating the $Ti_3C_2T_X$ sensor as a metallic channel and conducting a comparative analysis with BP, RGO, and MoS_2 for sensing various VOCs at room temperature. Utilizing the HF etching method, Kim and his team synthesized the $Ti_3C_2T_X$ sensor by replacing Al in the Ti_3AlC_2 powder through the LiF/HCl route. The resulting $Ti_3C_2T_X$ flakes exhibited high conductivity and were fully terminated with functional groups such as –OH, –O, and –F, as shown in Figure 10.

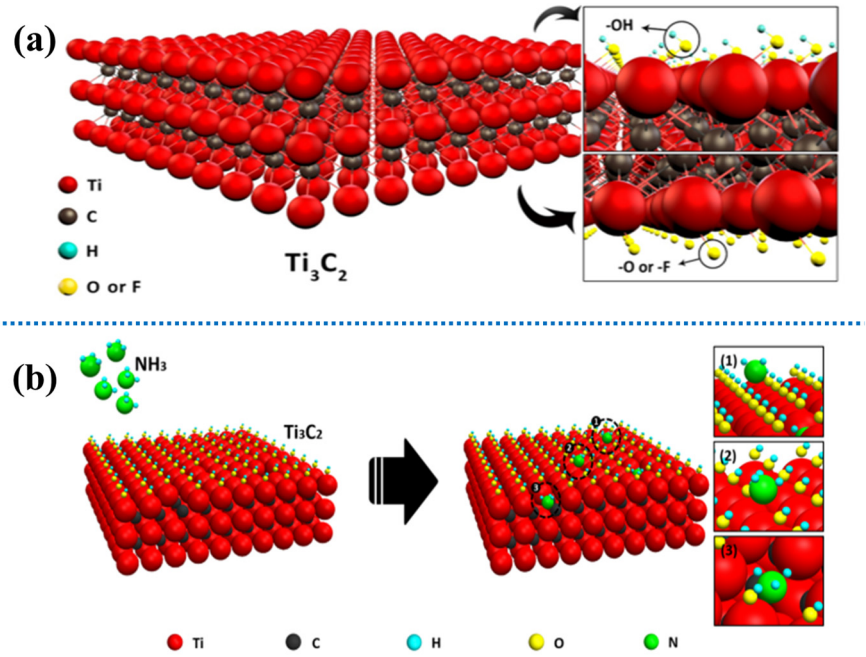

Figure 9. (**a**) Schematic representation of different functional groups attached at the surface of the Ti_3C_2 sensor. (**b**) A plausible gas sensing mechanism for ammonia over the Ti_3C_2 sensor [98].

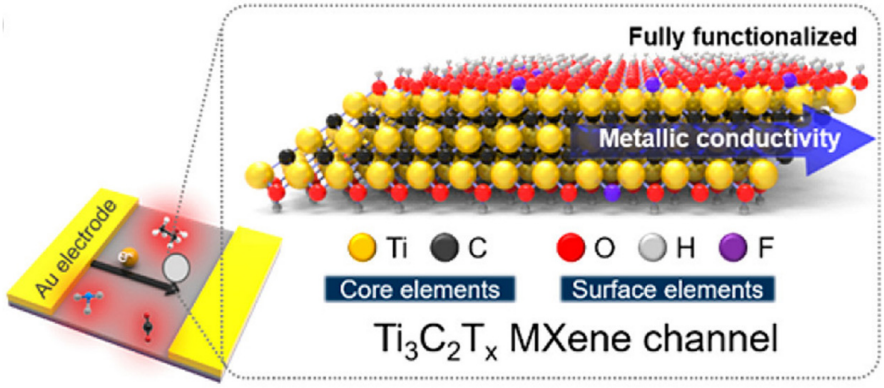

Figure 10. Schematic representation of atomic structure of $Ti_3C_2T_X$ film with different functional groups [99].

The fabricated –OH-functionalized $Ti_3C_2(OH)_2$ sensor demonstrated a very low detection limit of 50–100 ppb for VOCs at room temperature. This interesting combination resulted in highly attractive gas detection capabilities with an ultrahigh signal-to-noise ratio (SNR) when exposed to 100 ppm of ethanol, acetone, propanol, CO_2, NO_2, SO_2, and ammonia in real-time, as shown in Figure 11a. Among the different gases tested, ethanol exhibited the highest response of 1.7%, followed by propanol, and ammonia, whereas the sensor's response decreased towards some acidic gases like CO_2, NO_2, and SO_2, as shown in Figure 11a. The observed results suggest that $Ti_3C_2T_X$ exhibits high selectivity towards VOCs compared to acidic gases, attributed to its –OH group. This group plays a crucial role by forming hydrogen bonds with VOCs rather than in acidic gases. Additionally, the team compared the sensing performance of the prepared $Ti_3C_2T_X$ sensor with other 2D materials such as BP, MoS_2, and reduced graphene oxide (RGO). Figure 11b illustrates the real-time gas response of BP, MoS_2, RGO, and $Ti_3C_2T_X$ sensors towards 100 ppm of ethanol, acetone, and ammonia.

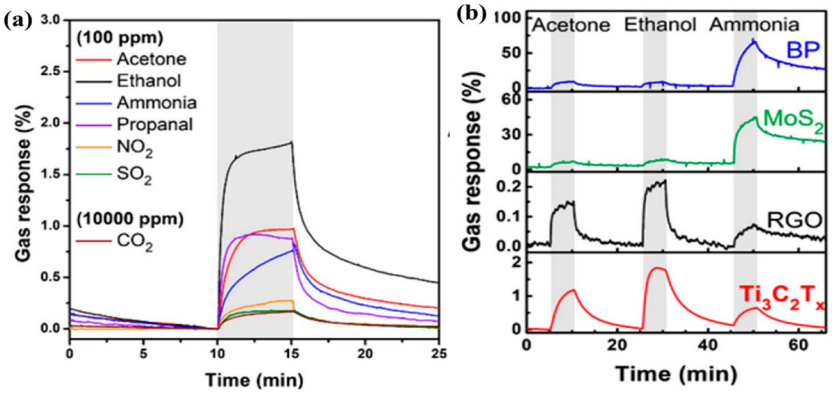

Figure 11. (**a**) Sensing performance of $Ti_3C_2T_X$ sensors at room temperature for 100 ppm of different analytes, and (**b**) real-time comparative gas sensing activity of $Ti_3C_2T_X$ sensors with other 2D materials upon exposure to 100 ppm of target analytes [99].

The gas sensing performance of MXenes have been observed to be influenced by precursor materials such as carbon sources, atoms, and the lateral dimension of the sheets. To investigate these effects, Christoper et al. utilized three commonly used carbon sources, graphite, TiC, and carbon lampblack, to synthesize Ti_3AlC_2 [100]. The synthesis of the Ti_3AlC_2 MAX phase was conducted at high temperature (1650 °C) for two hours using three different starting carbon sources, resulting in diverse morphologies and properties due to the distinct pathways, as shown in Figure 12a. The MAX phase synthesized using graphite as the carbon source exhibiting a flake size of up to 19.2 µm, while the MAX phase produced by the TiC precursor showed a flake size of 9.3 µm. Additionally, the MAX phase prepared using amorphous carbon lampblack showed a flake size of 2.4 µm, as shown in Figure 12b.

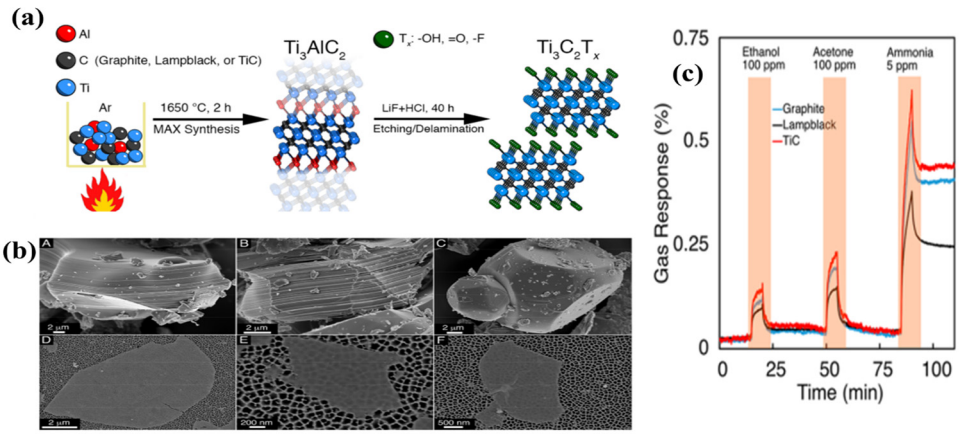

Figure 12. (**a**) Schematic illustration for the synthesis of Ti_3AlC_2 from different starting carbon precursors (graphite, lampblack and TiC) followed by the designing of the $Ti_3C_2T_X$ MAX phase using the HF etching route, (**b**) SEM photographs of Ti_3AlC_2 produced by (**A**) graphite, (**B**) TiC, and (**C**) carbon lampblack as carbon sources and fabrication of the $Ti_3C_2T_X$ MAX phase using a MILD-like process produced by (**D**) graphite, (**E**) TiC, and (**F**) carbon lampblack, and (**c**) the gas sensing activity of the $Ti_3C_2T_X$ MAX phase produced from different carbon sources towards ethanol, acetone, and ammonia [100].

They investigate the sensing performance of different MAX phases towards 100 ppm ethanol and acetone and 5 ppm of ammonia at room temperature [100]. Interestingly, the MAX phase obtained from smaller-sized flakes derived from amorphous carbon lampblack exhibited a lower gas response as compared to the MAX phase derived from graphite and TiC precursors, as shown in Figure 12c. In another study, Wu et al. developed a sensor based on a single layer Ti_3C_2 MXene for the selective detection of ammonia at room

temperature [89]. To prevent the formation of Li-ion residue on Ti_3C_2, they employed a different etching method, namely NaF + HCl, in contrast to the previously reported LiF + HCl etching route. This approach resulted in a clean surface, which facilitates the fast adsorption of ammonia due to the increased available area. After synthesis, they prepared a sensor by coating the surface of ceramic tubes with a colloidal suspension of a single layer of the Ti_3C_2 MXene for gas detection. The sensor was then exposed to various gases at a concentration of 500 ppm, such as CH_4, H_2O, NH_3, H_2S, NO, ethanol, methanol, and acetone. The Ti_3C_2 MXene-based sensor showed high selectivity for ammonia compared to other gases [89]. Tai and co-workers reported the synthesis of a Ti_3C_2Tx/γ-PGA gas sensor for NO_2 detection [101]. In their study, they demonstrated that modifying Ti_3C_2Tx with γ-poly(L-glutamic acid) (γ-PGA) significantly enhanced its gas sensing performance. This improvement is attributed to the unique synergistic interaction between γ-PGA and Ti_3C_2Tx, and the blocking effect facilitated by water molecules as well as increased effective adsorption of gas molecules. Additionally, their sensor exhibited fast response and recovery times, along with excellent stability. In another work, Tai's group developed a PANI/Nb_2CTx sensor for ammonia detection under humid conditions [90]. The fabricated PANI/Nb_2CTx sensor showed excellent gas sensing performance for ammonia concentrations as low as 0.1–10 ppm, with a detection limit of 20 ppb at 87.1% relative humidity. This superior performance is attributed to the various hydrogen bonds formed between polyaniline (PANI) and Nb_2CTx, resulting in superior selectivity, high sensitivity, and good long-term reliability, Furthermore, Tai's group also developed a V_2CTx MXene sensor for NO_2 detection [102]. Table 1 presents a summary of the gas sensing performance of different MXene-based sensors measured at room temperature.

Table 1. Gas sensing response of selected sensors based on different MXene structures at room temperature.

MXene	Analyte	Conc. (ppm)	Response	References
Ti_2CO_2	Ammonia	100		[94]
$Ti_3C_2T_X$	NH_3, Methanol, Ethanol, Acetone	100	0.21 0.143 0.115 0.075	[98]
$Ti_3C_2T_X$	NH_3, Propanol, Ethanol, Acetone, NO_2, SO_2, CO_2	100	0.8 0.88 1.7 0.97 0.25 0.2 0.1	[99]
$Ti_3C_2T_X$	NO_2	5	4.5%	[103]
$Ti_3C_2T_X$	Ethanol, Ammonia, Acetone	100 5 10	0.16 0.23 0.62	[100]
$Ti_3C_2T_X$	Acetone, Ethanol, Methanol, Ammonia, TCM, Water, NO_2	10 10 10 10 10,000 10,000 10	1.4 1.7 2.2 0.7 0.1 0.5 0.9	[104]

Table 1. *Cont.*

MXene	Analyte	Conc. (ppm)	Response	References
$Ti_3C_2T_X$	Ethanol, Acetaldehyde, Formaldehyde, Methanol, Methane, NO_2, Ammonia	100	2% 3% 5% 2% 4% 10% 28.87%	[105]
$Ti_3C_2T_X$	Ethanol CO_2	0.1%, 1%	35%, 0.5%	[106]
$Ti_3C_2T_X$	CH_4, H_2S, H_2O, Ethanol, Methanol, Acetone, Ammonia NO	500	0.5% 0.16% 0.37% 1.5% 0.2% 0.3% 6.13% 0.4%	[89]
V_2CT_X	Acetone, Methane, H_2, H_2S	100	0.0226 0.0167 0.2435 0.005	[107]
$V_4C_3T_X$	Acetone	100	2.5	[108]
Mo_2CT_X	Toluene	100	2.65%	[109]
α-Mo_2C	NO_2, Ammonia, Acetone, Propanal, Ethanol, Hexane, Toluene	5 5 1000	15% 4% 3% 4% 6% 1% 2%	[110]

3.2. Hybrid MXene-Based Gas Sensor

Significant work has been published for gas sensing utilizing pristine MXene-based sensors. However, their sensing abilities are still far away from the desired standards. The chemical and physical properties of pristine MXene, as well as its structure, greatly influence sensing performance. Therefore, strategies for improving gas sensing performance were realized by changing the carbon source of the MAX phase precursors, reducing the flake size, and increasing defect concentration. Further enhancement can be achieved by hybridizing pristine MXene with other materials to create synergistic effects between them. Designing hybrid composites offers a promising approach for improving sensitivity, selectivity, response/recovery times, and stability compared to pristine MXene, since MXene's higher specific surface area and other advantageous properties make it suitable for integration with a diverse array of materials. These include metal oxides semiconductors, TMDs, 2D materials (graphene), and organic polymers. Such hybridization not only improves their complexity but also enhances functionality, offering a wider spectrum of applications.

A lot of the published literature has focused on MOS due to their outstanding selectivity, sensitivity, and stability along with their ease of production and responsiveness to a diverse range of gases. Despite their merits, MOS typically needs some external stimuli, such as high temperature or UV light for activation, leading to increased costs, elevated power consumption, and risks of ignition with flammable gases. The combination of MOS with MXenes presents various advantages. MOS exhibit exceptional gas adsorption and catalytic characterization capabilities, while MXenes enhances electrical conductivity and offer a vast surface area for efficient gas adsorption. This combination enhances sensi-

tivity and selectivity towards different gasses. Tai et al. synthesized the MXene-based composite gas sensor ($TiO_2/Ti_3C_2T_X$) using in situ growth of TiO_2 nanowires on the Ti_3C_2 surface [111]. The designed composite sensor exhibits high sensitivity (1.63 times) and low response/recovery times (0.62/0.52) to 10 ppm ammonia at room temperature as compared to pristine MXene ($Ti_3C_2T_X$) [111]. In a separate study, He et al. used the hydrothermal approach to design an MXene decorated with SnO_2 nanoparticles [112]. The resulting MXene/SnO_2 composite heterojunction exhibited remarkable sensitivity and selectivity towards ammonia with a detection limit of 0.5 ppm at room temperature (Figure 13a). Moreover, the sensor exhibited rapid response and recovery times, both under 30 s, along with excellent stability (Figure 13b). Comparative analysis revealed that the sensor on the composite heterojunction outperformed pristine MXene by 40%, demonstrating n-type behavior [112]. The higher performance is attributed to an increased number of electrons on the SnO_2 surface due to difference in the Fermi levels of the MXene and SnO_2. Additionally, the composite structure provided selective adsorption abilities, further enhancing its functionality (Figure 13c,d). Wang et al. fabricated a composite comprising MXene ($Ti_3C_2T_X$) and WO_3 for NO_2 sensing using the electrospinning method [113]. Their $Ti_3C_2T_X/WO_3$ composite sensor exhibited excellent gas sensing activity towards different concentrations of NO_2 gas at room temperature (Figure 13e). The remarkable gas sensing response can be attributed to the higher electrical conductivity of both $Ti_3C_2T_X$ and WO_3 materials in air. Moreover, there was an accumulation of a greater number of electrons on the WO_3 surface due to the transfer of electrons from $Ti_3C_2T_X$ to WO_3, driven by the difference in Fermi levels (Figure 13f) [113]. Comparative analysis indicated that the gas sensing response of the composite sensor was 15 times higher than other reported chemiresistive-based sensors, such as MXene/WS_2 hybrids for 2 ppm NO_2 and $Ti_3C_2T_X/SnS_2$ for 1000 ppm NO_2 sensing [114,115].

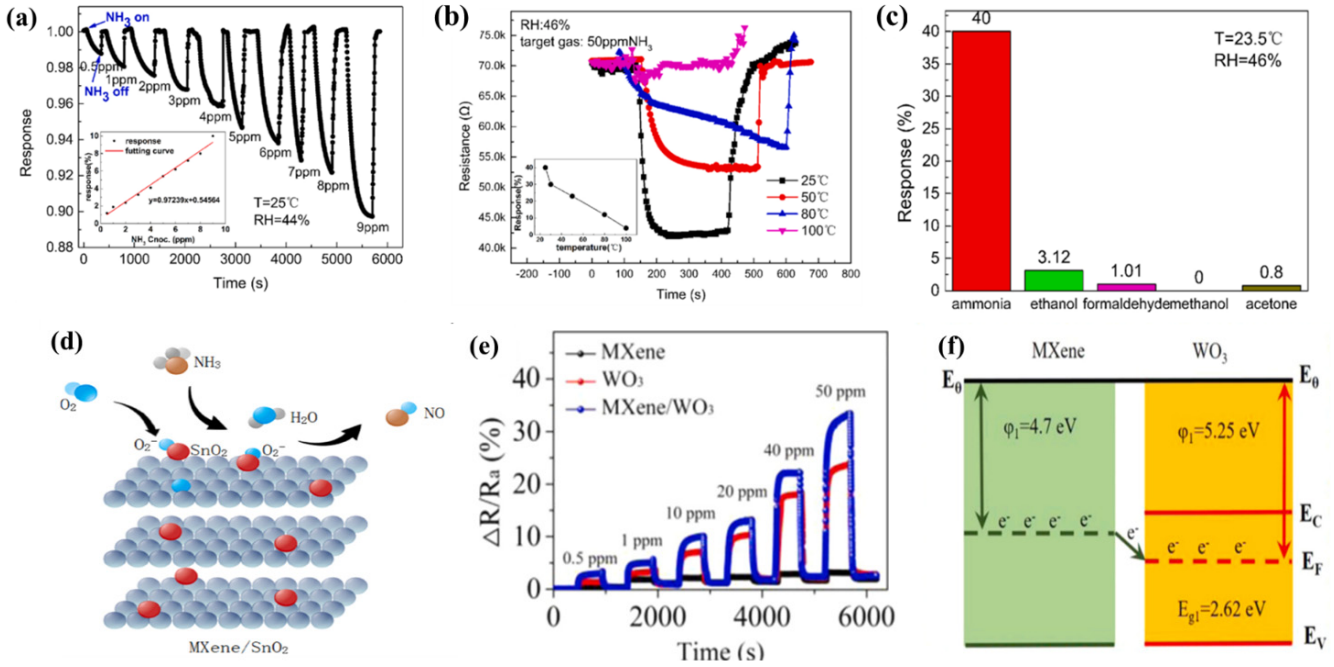

Figure 13. (**a**) The gas response of the MXene/SnO_2 sensor towards ammonia gas for different concentration (10–100 ppm) at room temperature, (**b**) the response and recovery times of the MXene/SnO_2 sensor towards 50 ppm ammonia at different temperatures, (**c**) the selectivity of MXene/SnO_2 towards ammonia in the presence of different analytes at room temperature, (**d**) the selective adsorption of ammonia on the MXene/SnO_2 sensor [112], (**e**) the sensing response variation ($\Delta R/R_a$) of MXene, WO_3, and MXene/WO_3 sensors for different concentrations of NO_2, and (**f**) a schematic presentation of the sensing mechanism and the transfer and accumulation of electrons at WO_3 [113].

The coupling of MXene with other 2D materials can offer a new platform for functionalizing hybrid materials. These hybrids can provide higher surface areas for gas adsorption, enhanced charge transfer capabilities, and improved electrical conductivity. Combining MXene with materials like graphene and other transition metal dichalcogenides provides distinct advantages, leading to superior sensing performance.

Tai and his co-workers also reported the synthesis of a hydride composite of MXene (Mo_2TiC_2Tx) with MoS_2 for NO_2 detection. Their study demonstrated that the Mo_2TiC_2Tx/MoS_2 gas sensor exhibited a superior response to NO_2, along with excellent selectivity against various interfering gases [116]. In another investigation, Tai's group reported the sensing of NO_2 using a V_2CTx/SnS_2 composite sensor at room temperature [117]. They demonstrated that the fabricated sensor exhibited NO_2 sensitivity 581.6 times higher than that of pristine V_2CTx. Lee et al. reported the development of a metal binder-free Ti_3C_2Tx/GO hybrid fiber for ammonia detection [93]. They demonstrated that the fabricated sensor exhibits an improved ammonia sensing response ($\Delta R/R_0$ = 6.77%) at ambient temperature as compared to MXene and graphene alone. This improvement is attributed to the synergistic impact of the electrical properties and gas adsorption capabilities of MXene and graphene. In other study, Tran et al. synthesized an rGO/Ti_3C_2Tx hybrid sensor using a simple ultrasonication method for NO_2 detection [118]. They showed that the developed sensor exhibited a sharp, large concentration-dependent, and cyclic response to NO_2 gas at room temperature. Moreover, the heterostructure showed excellent response to other toxic gases such as methane and toluene, outperforming other hybrid composites such as $MoS_2/Ti_3C_2T_x$ and g-$C_3N_4/Ti_3C_2T_x$, which were synthesized for comparison purposes [118].

Moreover, the formation of heterojunctions between MXene and polymers enhances mechanical flexibility and durability. Consequently, composite materials of MXene with polyaniline (PANI), Polypyrrole (PPy), Poly(3,4-ethylenedioxythiophene) polystyrene sulfonate (PEDOT-PSS), Polyethylenimine (PEI), etc., are attracting significant attention in sensor applications due to their high sensitivity and the low cost of polymers [119–122].

Li et al. developed a flexible chemiresistive gas sensor for ammonia detection based on a PANI/Ti_3C_2Tx hybrid film [119]. They reported that the sensor exhibited a low detection limit, high sensitivity, excellent repeatability, and good stability in air. These attributes were attributed to the Schottky junction and improved protonation degree of PANI in the hybrid composite. Similarly, Shen and co-workers synthesized a hybrid nanocomposite of PPy and MXene using a simple in situ polymerization approach for ammonia sensing [120]. They found that the PPy/Mxene-12 sensor demonstrated excellent response to 100 ppm ammonia at room temperature, which was 2.38 and 6.38 times higher than that of PPy and MXene, respectively. Additionally, the sensor showed excellent selectivity with a low detection limit. Chu and coworkers synthesized a PEDOT:PSS/MXene hybrid composite sensor using a dip coating technique for ammonia sensing [121]. The fabricated sensor shows a strong response to 100 ppm ammonia at room temperature, with fast response and recovery times of 116 and 40 s, respectively. They attributed the improved sensing performance to the synergistic effect between the PEDOT:PSS polymer and the Ti_3C_2Tx MXene. In another study, Zhou et al. synthesized the nitrogen-doped Ti_3C_2Tx MXene/polyethyleneimine composite films decorated with reduced graphene oxide nanosheets for CO_2 sensing [122]. They reported that the fabricated ternary sensor with a PEI loading of 0.001 mg/mL exhibited reversible and superior performance compared to other counterparts at room temperature. Moreover, the sensor demonstrated favorable repeatability, selectivity, a low detection limit of 8 ppm, and long-term stability. Table 2 shows the reported performance of gas sensors using MXenes [90,115,123–130].

Table 2. Gas sensing responses of selected sensors based on hybrids of MXenes at room temperature.

MXene Hybrid	Analyte	Conc. (ppm)	Response	References
Ti_3C_2Tx/TiO_2	NO_2	10	1.9%	[123]
$Ti_3C_2T_X/CuO$	Toluene	50	11.4%	[124]
$Ti_3C_2T_X/WSe_2$	Ethanol	40	12%	[125]
$Ti_3C_2T_X/ZnO$	NO_2	100	41.9%	[126]
$Ti_3C_2T_X/SnO\text{-}SnO_2$	Acetone	100	12.1%	[126]
$Ti_3C_2T_X/ZnSnO_3$	Formaldehyde	100	194.7%	[127]
$Ti_3C_2T_X/In_2O_3$	Methanol	5	29.6%	[128]
$Ti_3C_2T_X/\alpha\text{-}Fe_2O_3$	Acetone	5	16.6%	[129]
$Ti_3C_2T_X$/Graphene fibers	Ammonia	100	6.77%	[129]
Nb_2CTx/PANI	Ammonia	100	1.19%	[90]
$Ti_3C_2T_X$/Poly glutamic acid	NO	50	1127.3%	[90]
Ti_3C_2Tx/WS_2	NO	100	76.9%	[115]
Nb_2CTx/PANI	Ammonia	100	301.31%	[130]

4. MXene-Based Optical Sensors

MXene-based materials have emerged as one of the most captivating materials within the realm of 2D materials, owing to their distinctive array of properties. These include facile surface functionalization, high conductivity, outstanding hydrophilicity, extensive surface area, biocompatibility, and superior optical characteristics, alongside its promising potential for employment in biosensing applications. MXenes exhibit versatility in their forms, ranging from quantum dots to composite structures and nanosheets, achieved through various synthesis methods and appropriate etching techniques. Over the past few years, MXene has garnered attention for its application in wearable sensors, electrochemical sensors, and optical biosensors.

MXenes have rapidly emerged as a prominent category within the realm of 2D materials, owing to their exceptional mechanical, electronic, and electrical properties. The interplay between the structural and electronic characteristics of MXenes is intimately tied to their optical behavior. Specifically, transitions between electronic bands can significantly enhance the optical response at specific wavelengths. Investigating optical properties involves a thorough examination of factors such as the lattice structure of MXenes, surface modifications, and elemental compositions. Various research studies are published to explore the physicochemical properties (optical properties, including reflectivity, transmittance, plasmon resonance, and absorption) of the MXenes and their hybrid composite materials. The electronic band structure, particularly the energy bandgap, plays a pivotal role in shaping these optical characteristics. For instance, MXenes with higher electronegative terminations, such as –O, tend to exhibit wider bandgaps compared to terminations like –F and –OH [48]. Thus, it is expected that MXenes with wide band gaps can be used for photocatalytic applications under UV light irradiation. In contrast, MXenes with narrow band gaps can be utilized as visible light photocatalysts for water treatment and photocatalytic hydrogen evolution reactions.

Theoretical approaches, notably density functional theory (DFT), have been instrumental in predicting MXenes' optical response. Initial DFT investigations focused on determining the band structure and density of states for various MXene compositions, such as Ti_2N, Ti_3C_2, TiC_2, and Ti_3N_2 [131]. These studies revealed favorable energy bandgaps within the visible light range, suggesting potential applications in photocatalysis and light-driven processes [132]. Experimental findings complement theoretical predictions, demonstrating MXenes' remarkable optical properties. For example, delaminated $Ti_3C_2T_x$

films and $Ti_3C_2T_x$ intercalated with NH_4HF_2 structures exhibit high transmittance levels, reaching up to 77% in the visible region and even 90% extending into the infrared spectrum [42,133]. Moreover, the optical response of MXenes varies with the number of layers, and optimization strategies, including thickness variation and ion intercalation, have been explored to optimize transmittance [28,133]. Studies have also highlighted the reversible changes in transmittance observed during electrochemical intercalation processes, particularly within the UV–visible range. Additionally, variations in flake size impact the optical absorption spectra of $Ti_3C_2T_x$, further emphasizing the nuanced relationship between MXene structure and optical behavior [134]. The reduction in size of MXene flakes correlates with a decrease in absorbance values at 237 nm, whereas larger flakes exhibit higher absorbance at 375 nm. This suggests a decrease in absorption within the visible range as flake size diminishes. However, despite this optical trend, smaller flakes demonstrate superior electrochemical performance with higher capacitance, likely due to enhanced electrolyte accessibility to active sites, thus conflicting with optical properties [135]. Surface functionalization, such as with –F, –O, and –OH groups, could passivate MXene layers, offering a means to control both electronic and optical properties [136]. Computational studies utilizing DFT have been employed to observe the effects of surface termination groups (–F, –O, and –OH) on the optical properties of $Ti_3C_2T_2$ [137]. In the visible range, O-functionalized MXene exhibits higher absorption and reflectivity compared to unfunctionalized MXene, while –F- and –OH-functionalized MXene display lower absorption. Conversely, in the UV range, all –F-, –O-, and –OH-functionalized MXenes demonstrate enhanced absorption [137]. Similarly, in $Ti_3C_2T_2$ and Ti_2CT_2, –O termination shows superior light absorption in the UV range compared to –F and –OH terminations, possibly attributed to the formation of states near the Fermi energy level [137,138]. Optical sensors have garnered significant attention due to their diverse applications ranging from food processing control, drug discovery, environmental monitoring, therapeutics, and clinical diagnostics. Transduction elements in sensing systems leverage phenomena such as light scattering, fluorescence/phosphorescence, light absorption, Raman scattering, and surface plasmon resonance (SPR). With the burgeoning growth of nanotechnology, 2D materials like graphene and MXenes have witnessed remarkable utilization in sensing applications owing to their unique properties including colorimetry, photoluminescence, electrochemiluminescence (ECL), surface-enhanced Raman scattering (SERS), and SPR. Various forms of MXenes, including quantum dots and nanosheets, are elucidated herein alongside their diverse applications [138].

4.1. Colorimetric Sensors

Notably, colorimetric sensors, renowned for their simplicity, cost-effectiveness, and high selectivity/sensitivity, have capitalized on MXene nanocomposites for sensor fabrication. Based on the visualization of a nano-plasmonic strategy, Wang et al. developed Ti_3C_2 MXenes for label-free and visual sensing of silver ions, exploiting the reductive and adsorptive properties of silver towards MXene to form plasmonic silver nanoparticles conducive to silver sensing [139].

In another study, Li et al. [140] proposed the sensing properties of the Ti_3C_2/CuS nanocomposites for the determination of cholesterol. An SEM image of the synthesized Ti_3C_2/CuS nanocomposites is shown in Figure 14a. It can be seen that the Ti_3C_2 MXene is attached to the CuS. The synthetic process and probable oxidation of cholesterol is displayed in Figure 14b. Ti_3C_2/CuS nanocomposites have demonstrated peroxidase-like activity for cholesterol detection via a colorimetric method, achieving a LOD of 1.9 μM [140].

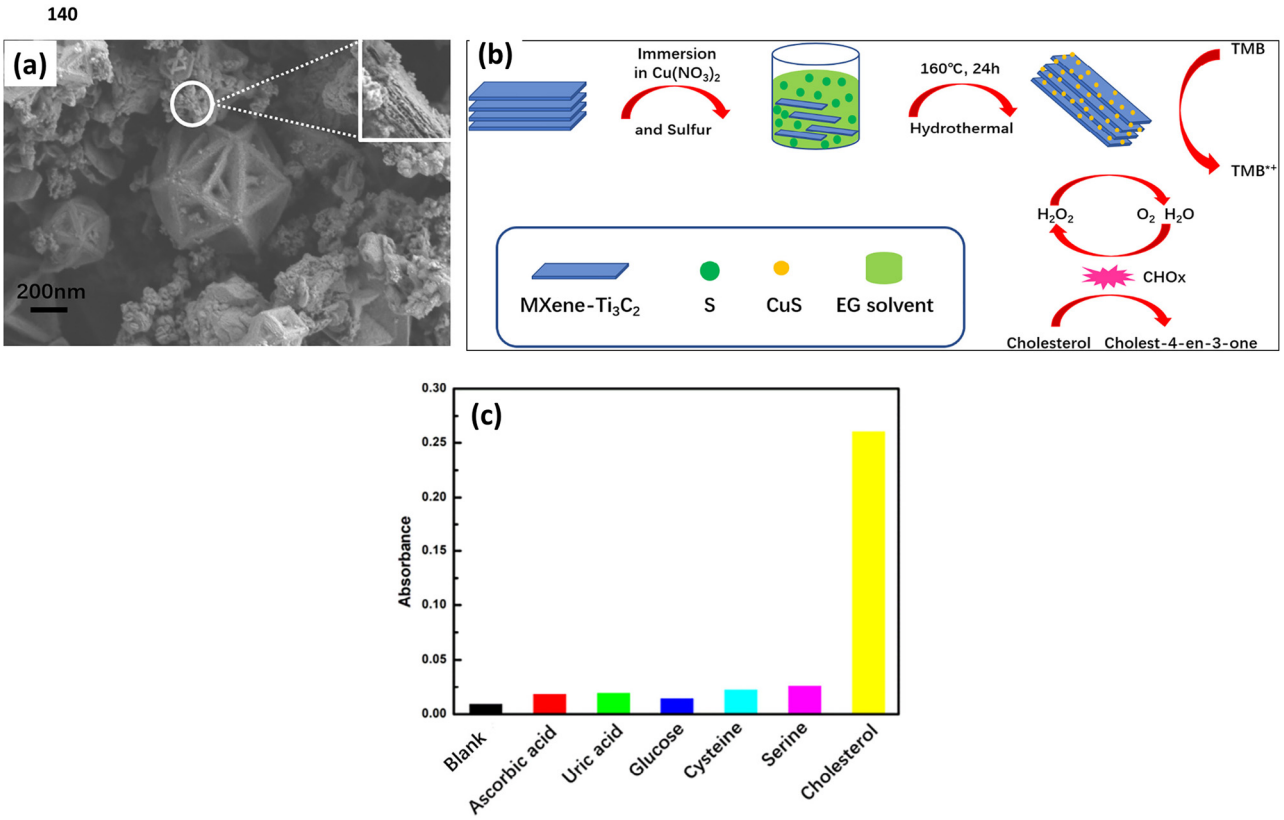

Figure 14. (**a**) The SEM image and the schematic illustration (**b**) of the preparation of Ti_3C_2/CuS nanocomposites. (**c**) Selectivity of Ti_3C_2/CuS nanocomposites for cholesterol sensing [140].

The colorimetric change from colorless to blue, catalyzed by the nanocomposite in the presence of hydrogen peroxide and 3,3,5,5-tetramethylbenzidine, correlates with cholesterol concentration in the solution. The Ti_3C_2/CuS nanocomposites are also highly selective towards the detection of cholesterol, as shown in Figure 14c. Furthermore, a 2D heterojunction hybrid combining a Ni-Fe-layered double hydroxide and $Ti_3C_2T_x$ MXene nanosheets has been designed for colorimetric sensing of glutathione in human serum [141]. This hybrid enhances electron transfer rates and offers increased surface area for ion interaction, thereby exhibiting heightened peroxidase-like catalytic activity.

Additionally, Prussian blue-functionalized $Ti_3C_2T_x$ composites have been utilized for colorimetric sensing of pesticides and H_2O_2 [142]. The immobilization of acetylcholinesterase on Prussian blue-functionalized $Ti_3C_2T_x$-modified electrodes enables the electrochemical sensing of malathion. Similarly, thrombin detection in blood samples has been achieved based on the peroxidase mimicking the nanozyme activity of $Ti_3C_2T_x$ MXenes, wherein adsorption of ssDNA on Ti_3C_2 nanosheets enhances the catalytic activity for sensing, while the presence of thrombin leads to aptamer detection on the nanosheet surface, accompanied by a decrease in catalytic activity [143].

4.2. Surface Plasmon Resonance (SPR) Sensors

Surface plasmon resonance (SPR) technology has revolutionized sensing approaches in various fields such as food safety, energy storage, optics, and medical diagnostics [144]. Due to their rapid response and high sensitivity, MXene-based SPR sensors have garnered significant attention from researchers. Xu et al. proposed a theoretical design for an MXene-based SPR sensor, combining transition metal dichalcogenides with the Ti_3C_2 MXene [145]. They achieved higher refractive index sensitivity in aqueous solutions using a five-layer WS_2 and monolayer $Ti_3C_2T_x$ MXene setup excited at a wavelength of 633 nm. This setup demonstrated enhanced sensitivity compared to conventional bare Au-based

SPR sensors. Moreover, Srivastava et al. [146] demonstrated the theoretical possibility of designing SPR sensors by combining transition metal dichalcogenides, Ti_3C_2 MXene, black phosphorus, and Au. The authors recorded the highest sensitivity using a single layer of the $Ti_3C_2T_x$ MXene nanomaterial, with a penetration depth 1.52 times higher than conventional Au sensors.

In the development of fiber optic-based sensors, graphene-like materials have been used instead of transition metal dichalcogenides. An SPR sensor based on Au/graphene/Ti_3C_2 was developed for volatile organic compound detection [147]. The combination of metals and varying numbers of MXene and graphene layers has proven effective in sensor development, with the refractive index of the sensor varying according to solvent variation. Additionally, an SPR biosensor employing black phosphorus and $Ti_3C_2T_x$ layers has been developed for gas and biosensing applications [148]. The thickness and atomic layer numbers of MXene are crucial as they interact with specific biomolecules, providing a platform for SPR-based biosensing. Wu et al. [149] synthesized Au-decorated Ti_3C_2 MXene nanosheets and its formation was confirmed by the XRD technique. The authors found that the Ti_3C_2 MXene and Ti_3C_2 MXene/AuNPs were successfully formed, as shown in Figure 15a.

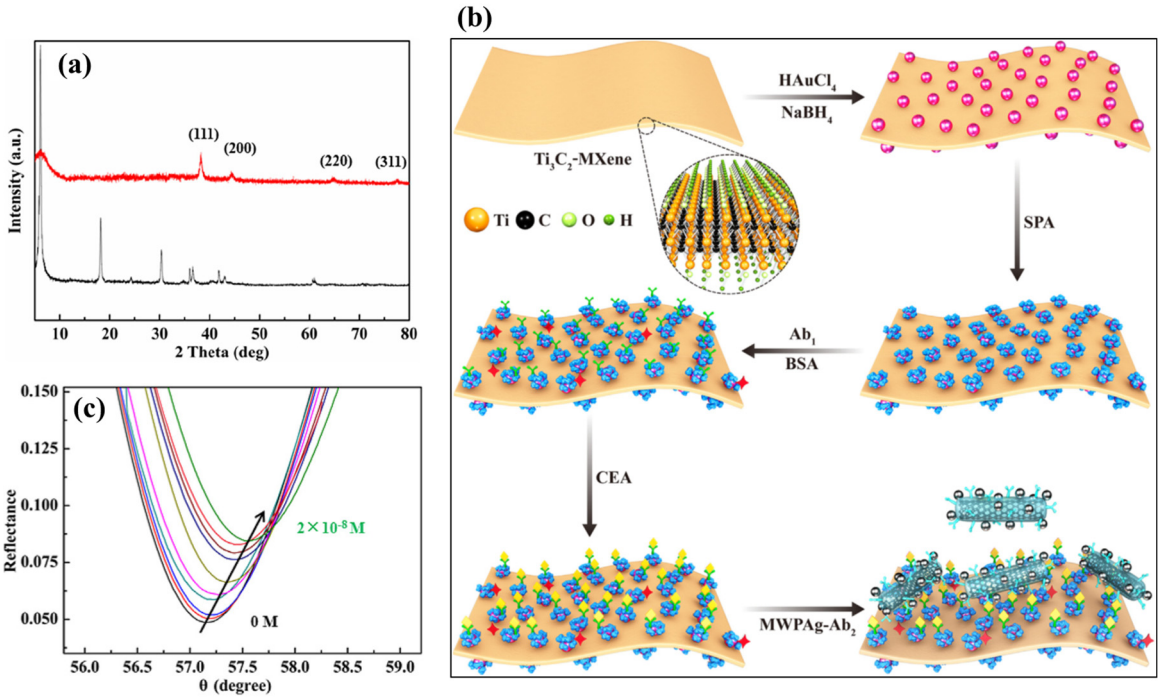

Figure 15. (**a**) XRD patterns of Ti_3C_2 MXene and Ti_3C_2 MXene/AuNPs. (**b**) Schematic diagram for the preparation of biosensors. (**c**) SPR spectra of CEA at different concentrations (2×10^{-16}–2×10^{-8} M) with the proposed biosensor [149].

Furthermore, an ultrasensitive SPR biosensor for the detection of carcinoembryonic antigen (CEA) was developed as shown in Figure 15b. The SPR spectra of CEA in the presence of different concentrations (2×10^{-16}–2×10^{-8} M) is presented in Figure 15c. It is clearly shown that the proposed sensor has good sensing activity with a decent linear range. The proposed biosensor exhibited an LOD of 0.07 fM. In another approach, CEA detection based on an SPR sensor was achieved by immobilizing amine-functionalized Ti_3C_2-AuNPs-SPA with polyclonal anti-CEA antibodies, achieving a LOD of 0.15 fM [150]. This new approach for detecting biomolecules in complex mixtures has demonstrated good selectivity, as evidenced by the high recoveries of spiked blank serum samples.

4.3. Surface-Enhanced Raman Scattering

Raman spectroscopy has emerged as a powerful analytical tool for the easy identification and interpretation of trace amounts of chemicals due to their unique vibrational characteristics. When light of a specific wavelength interacts with the surface of materials, it produces oscillations, generating enhanced signals known as surface-enhanced Raman scattering (SERS) signals [151]. MXenes provide a flexible environment as SERS substrates, owing to their hydrophilic nature, optical properties, and large surface area, making them promising for SERS with excellent stability and selectivity. Several MXene-based SERS approaches have been reported for sensing pollutants such as pesticides and dyes. For instance, a hybrid composite of the $Ti_3C_2T_x$ MXene with silver, gold, and platinum nanoparticles has been used in SERS-based sensors for the detection of methylene blue [152]. Furthermore, the $Ti_3C_2T_x$ MXene has been individually explored as a SERS substrate for the effective sensing of organic dyes like Rhodamine 6G [153]. SERS signals in MXenes are observed due to inter-band transitions of vacant energy states, followed by charge transfer. Similarly, SERS signals of two-dimensional transition metal nitrides (Ti_2N) have been verified by fabricating them on silicon, paper, and glass-based SERS substrates. A paper-based Ti_2N MXene-based SERS substrate has been utilized for the detection of trace-level explosives [154]. In another approach, Au nanorods immobilized on the $Ti_3C_2T_x$ MXene were synthesized for the detection of organic pollutants such as Rhodamine 6G, malachite green, and crystal violet on SERS-based sensors. The Au nanorods distribute uniformly on MXene via strong electrostatic interactions, exhibiting high sensitivity and good reproducibility. The synergic connection between the charge transfer of MXene and resonance Raman scattering enables the detection of single molecules of pollutants [155].

Zheng et al. [156] synthesized a SERS aptasensor based on an internal standard approach for the sensitive detection of Ochratoxin A. Au–Ag Janus nanoparticles accumulate with MXene via H-bonding, and chelation interactions occur between MXene and OTA aptamers. In the presence of OTA, the Au–Ag Janus nanoparticles separate from MXene due to the formation of the OTA/aptamers complex, leading to Raman signal generation. Medetalibeyoglu et al. [157] developed an ultra-sensitive carcinoembryonic antigen sensor using Fe_3O_4@Au nanoparticles functionalized with MXene as a SERS substrate.

Figure 16a,b show the SEM picture of the d-$Ti_3C_2T_X$ MXene and Fe_3O_4 NPs@Au NPs/d-$Ti_3C_2T_X$ MXene, respectively. It is clearly seen that the Fe_3O_4 NPs@Au NPs are strongly attached to the surface of the d-$Ti_3C_2T_X$ MXene. Furthermore, the authors investigated the sensing activities of the proposed material and found that the fabricated sensor is selective towards the determination of CEA, as shown in Figure 16c. The interesting LOD of 0.033 pg mL^{-1} was reported for the above proposed sensor. It is clear that the Fe_3O_4 NPs@Au NPs/d-$Ti_3C_2T_X$ MXene has a selective nature for the sensing of CEA with decent LOD. Table 3 summarizes the utilization of MXene and its composite materials in various optical sensing applications.

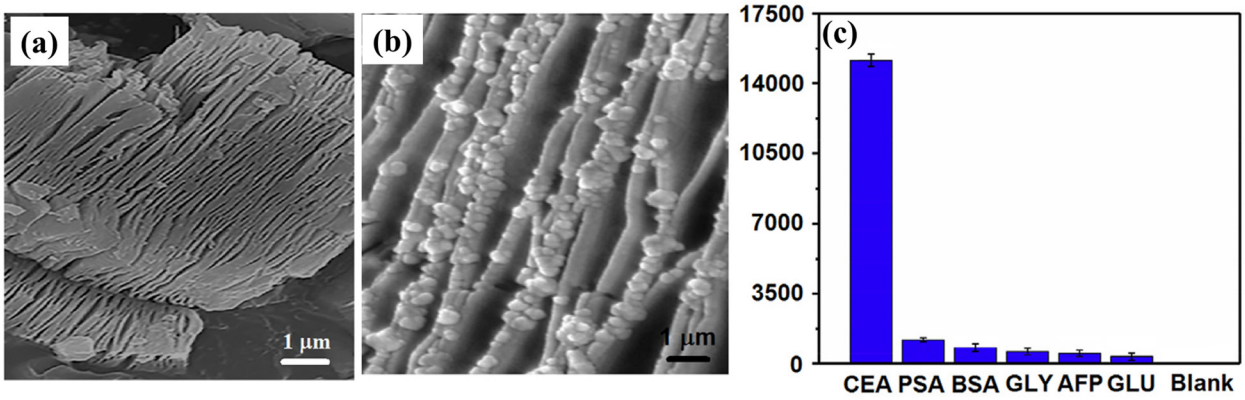

Figure 16. (**a**) SEM image of d-$Ti_3C_2T_X$ MXene and (**b**) Fe_3O_4 NPs@Au NPs/d-$Ti_3C_2T_X$ MXene. (**c**) SERS intensity of different antigens [157].

Table 3. Utilization of MXenes as optical sensors for the detection of various biomolecules and hazardous materials.

Material	Type of Sensor	Detection	Reference
Ti_3C_2 MXenes	Colorimetric	Ag^+	[139]
Ti_3C_2/CuS nanocomposites	Colorimetric	Cholesterol	[140]
$Ti_3C_2T_x$ MXene	Colorimetric	Glutathione	[141]
$Ti_3C_2T_x$ composites	Colorimetric	Pesticides and H_2O_2	[142]
$Ti_3C_2T_x$	Colorimetric	Thrombin	[143]
Au/graphene/Ti_3C_2	SPR Sensor	Organic compound	[147]
Black phosphorus and $Ti_3C_2T_x$	SPR Sensor	Gas and biosensing	[148]
Ti_3C_2-AuNPs-SPA	SPR Sensor	CEA	[149]
$Ti_3C_2T_x$ hybrid composite	SERS	Methylene blue	[152]
$Ti_3C_2T_x$	SERS	Rhodamine 6G	[153]
Ti_2N MXene	SERS	Explosives	[154]
Au nanorod-immobilized $Ti_3C_2T_x$	SERS	Rhodamine 6G, malachite green, and crystal violet	[155]
Fe_3O_4@Au nanoparticle-functionalized MXene	SERS	Carcinoembryonic antigen	[157]

5. Conclusions and Future Perspectives

In conclusion, this review article has summarized the recent advancements in the fabrication of gas sensors and optical sensors using MXenes. MXenes exhibit excellent properties that make them promising candidates for fabricating gas sensors and biosensors. Numerous gas sensors have been demonstrating outstanding performance in terms of detection limit. MXenes are perfect for the selective and precise detection of different gases at room temperature due to their high surface area, excellent conductivity, and adaptable surface chemistry. Moreover, composites of MXenes significantly enhance the specific surface area, expand interlayer spacing, and introduce new active sites for gas adsorption. Therefore, modifying MXenes with different materials can improve gas sensing performance, including selectivity, gas response and recovery times, as well as detection limit. This highlights the synergetic effects of the MXene and its composites. These properties underscore MXenes' desirability in the development of high-performance sensing devices. Similarly, various studies have highlighted the potential of MXenes in the fabrication of optical sensors. While MXenes and their hybrid materials have been utilized in gas and optical sensors construction, their application in detecting toxic gases through gas sensing technology is noteworthy. MXene-based sensors and their composite derivatives are currently in the early stages of development. Although approximately 20 types of MXenes have been synthesized, only a few, particularly $Ti_3C_2T_x$, have been extensively explored for sensing applications. However, there are some drawbacks that need to be addressed to expand their gas sensing capabilities. These include the low hydrophilicity in multilayer MXenes, high metallic conductivity, low flexibility, and challenges with decomposition and oxidation stability. Additionally, they also exhibit slow response and recovery times, attributed to sluggish kinetics at low temperatures. To overcome these challenges, significant efforts are required to enhance the sensing performance. This can be achieved through optimizing flake size and morphology, choosing better surface termination, and exploring the fabrication of hybrid materials. Moreover, to expand the application of MXenes in various real-time applications, reducing production costs and focusing on computational predictions, along with generating experimental data, are crucial steps for future studies. Research should advance beyond individual evaluations of MXene sensors' selectivity and

sensitivity for particular gases or VOCs. There should be shifted towards more focused applications such as human health monitoring, non-invasive disease diagnosis, and the detection of hazardous and toxic gases in real-world environments.

Funding: This research received no external funding.

Acknowledgments: P.K. gives thanks to DST-Inspire, New Delhi, India, for providing funding for his PhD fellowship.

Conflicts of Interest: The authors declare no conflict of interest.

References

1. Dutta, T.; Yadav, N.; Wu, Y.; Cheng, G.J.; Liang, X.; Ramakrishna, S.; Sbai, A.; Gupta, R.; Mondal, A.; Hongyu, Z.; et al. Electronic Properties of 2D Materials and Their Junctions. *Nano Mater. Sci.* **2024**, *6*, 1–23. [CrossRef]
2. Thakur, N.; Kumar, P.; Kumar, S.; Singh, A.K.; Sharma, H.; Thakur, N.; Dahshan, A.; Sharma, P. A Review of Two-Dimensional Inorganic Materials: Types, Properties, and Their Optoelectronic Applications. *Prog. Solid State Chem.* **2024**, *74*, 100443. [CrossRef]
3. Raza, W.; Ahmad, K.; Kim, H. Fabrication of Defective Graphene Oxide for Efficient Hydrogen Production and Enhanced 4-Nitro-Phenol Reduction. *Nanotechnology* **2021**, *32*, 495404. [CrossRef]
4. Ahmad, K.; Kim, H. Hydrothermally Synthesized $MoSe_2$/rGO Composite as Electrode Modifier for the Construction of Non-Enzymatic Urea Sensor. *Mater. Chem. Phys.* **2022**, *286*, 126206. [CrossRef]
5. Yang, F.; Cheng, S.; Zhang, X.; Ren, X.; Li, R.; Dong, H.; Hu, W. 2D Organic Materials for Optoelectronic Applications. *Adv. Mater.* **2018**, *30*, 1702415. [CrossRef]
6. Cheng, J.; Wang, C.; Zou, X.; Liao, L. Recent Advances in Optoelectronic Devices Based on 2D Materials and Their Heterostructures. *Adv. Opt. Mater.* **2019**, *7*, 1800441. [CrossRef]
7. Zhao, M.; Hao, Y.; Zhang, C.; Zhai, R.; Liu, B.; Liu, W.; Wang, C.; Jafri, S.H.M.; Razaq, A.; Papadakis, R.; et al. Advances in Two-Dimensional Materials for Optoelectronics Applications. *Crystals* **2022**, *12*, 1087. [CrossRef]
8. Ma, Q.; Ren, G.; Mitchell, A.; Ou, J.Z. Recent Advances on Hybrid Integration of 2D Materials on Integrated Optics Platforms. *Nanophotonics* **2020**, *9*, 2191–2214. [CrossRef]
9. Mishra, R.K.; Sarkar, J.; Verma, K.; Chianella, I.; Goel, S.; Nezhad, H.Y. Borophene: A 2D Wonder Shaping the Future of Nanotechnology and Materials Science. *Nano Mater. Sci.* 2024; *in press*. [CrossRef]
10. Shim, J.; Park, H.-Y.; Kang, D.-H.; Kim, J.-O.; Jo, S.-H.; Park, Y.; Park, J.-H. Electronic and Optoelectronic Devices Based on Two-Dimensional Materials: From Fabrication to Application. *Adv. Electron. Mater.* **2017**, *3*, 1600364. [CrossRef]
11. Avouris, P.; Dimitrakopoulos, C. Graphene: Synthesis and Applications. *Mater. Today* **2012**, *15*, 86–97. [CrossRef]
12. Wang, Q.H.; Kalantar-Zadeh, K.; Kis, A.; Coleman, J.N.; Strano, M.S. Electronics and Optoelectronics of Two-Dimensional Transition Metal Dichalcogenides. *Nat. Nanotechnol.* **2012**, *7*, 699–712. [CrossRef]
13. Khan, M.F.; Ahmed, F.; Rehman, S.; Akhtar, I.; Rehman, M.A.; Shinde, P.A.; Khan, K.; Kim, D.; Eom, J.; Lipsanen, H.; et al. High Performance Complementary WS_2 Devices with Hybrid Gr/Ni Contacts. *Nanoscale* **2020**, *12*, 21280–21290. [CrossRef] [PubMed]
14. Xu, M.; Liang, T.; Shi, M.; Chen, H. Graphene-Like Two-Dimensional Materials. *Chem. Rev.* **2013**, *113*, 3766–3798. [CrossRef] [PubMed]
15. Xia, F.; Wang, H.; Xiao, D.; Dubey, M.; Ramasubramaniam, A. Two-Dimensional Material Nanophotonics. *Nat. Photon.* **2014**, *8*, 899–907. [CrossRef]
16. Vu, Q.A.; Yu, W.J. Electronics and Optoelectronics Based on Two-Dimensional Materials. *J. Korean Phys. Soc.* **2018**, *73*, 1–15. [CrossRef]
17. Mannix, A.J.; Kiraly, B.; Hersam, M.C.; Guisinger, N.P. Synthesis and Chemistry of Elemental 2D Materials. *Nat. Rev. Chem.* **2017**, *1*, 14. [CrossRef]
18. Ahmad, K.; Kim, H. Fabrication of Nickel-Doped Tungsten Trioxide Thin Film-Based Highly Stable Flexible Electrochromic Devices for Smart Window Applications. *ACS Sustain. Chem. Eng.* **2023**, *11*, 10746–10754. [CrossRef]
19. Quasim Khan, M.; Alharthi, F.A.; Ahmad, K.; Kim, H. Hydrothermal Synthesis of $BaTiO_3$ Perovskite for H_2O_2 Sensing. *Chem. Phys. Lett.* **2022**, *805*, 139950. [CrossRef]
20. Khan, M.Q.; Kumar, P.; Khan, R.A.; Ahmad, K.; Kim, H. Fabrication of Sulfur-Doped Reduced Graphene Oxide Modified Glassy Carbon Electrode (S@rGO/GCE) Based Acetaminophen Sensor. *Inorganics* **2022**, *10*, 218. [CrossRef]
21. Li, Y.; Fu, J.; Mao, X.; Chen, C.; Liu, H.; Gong, M.; Zeng, H. Enhanced Bulk Photovoltaic Effect in Two-Dimensional Ferroelectric $CuInP_2S_6$. *Nat. Commun.* **2021**, *12*, 5896. [CrossRef]
22. Liu, M.; Yin, X.; Ulin-Avila, E.; Geng, B.; Zentgraf, T.; Ju, L.; Wang, F.; Zhang, X. A Graphene-Based Broadband Optical Modulator. *Nature* **2011**, *474*, 64–67. [CrossRef]
23. Razaq, A.; Bibi, F.; Zheng, X.; Papadakis, R.; Jafri, S.H.M.; Li, H. Review on Graphene-, Graphene Oxide-, Reduced Graphene Oxide-Based Flexible Composites: From Fabrication to Applications. *Materials* **2022**, *15*, 1012. [CrossRef] [PubMed]
24. Naguib, M.; Kurtoglu, M.; Presser, V.; Lu, J.; Niu, J.; Heon, M.; Hultman, L.; Gogotsi, Y.; Barsoum, M.W. Two-Dimensional Nanocrystals Produced by Exfoliation of Ti_3AlC_2. In *MXenes*; Jenny Stanford Publishing: Singapore, 2023; ISBN 978-1-00-330651-1.

25. Anasori, B.; Xie, Y.; Beidaghi, M.; Lu, J.; Hosler, B.C.; Hultman, L.; Kent, P.R.C.; Gogotsi, Y.; Barsoum, M.W. Two-Dimensional, Ordered, Double Transition Metals Carbides (MXenes). *ACS Nano* **2015**, *9*, 9507–9516. [CrossRef] [PubMed]
26. Akhter, R.; Maktedar, S.S. MXenes: A Comprehensive Review of Synthesis, Properties, and Progress in Supercapacitor Applications. *J. Mater.* **2023**, *9*, 1196–1241. [CrossRef]
27. Dahlqvist, M.; Barsoum, M.W.; Rosen, J. MAX Phases—Past, Present, and Future. *Mater. Today* **2024**, *72*, 1–24. [CrossRef]
28. Deysher, G.; Shuck, C.E.; Hantanasirisakul, K.; Frey, N.C.; Foucher, A.C.; Maleski, K.; Sarycheva, A.; Shenoy, V.B.; Stach, E.A.; Anasori, B.; et al. Synthesis of Mo_4VAlC_4 MAX Phase and Two-Dimensional Mo_4VC_4 MXene with Five Atomic Layers of Transition Metals. *ACS Nano* **2020**, *14*, 204–217. [CrossRef] [PubMed]
29. Ouadha, I.; Rached, H.; Azzouz-Rached, A.; Reggad, A.; Rached, D. Study of the Structural, Mechanical and Thermodynamic Properties of the New MAX Phase Compounds $(Zr_{1-x}Tix)_3AlC_2$. *Comput. Condens. Matter* **2020**, *23*, e00468. [CrossRef]
30. Gogotsi, Y.; Anasori, B. The Rise of MXenes. *ACS Nano* **2019**, *13*, 8491–8494. [CrossRef] [PubMed]
31. Javaid, M.; Haleem, A.; Singh, R.P.; Rab, S.; Suman, R. Significance of Sensors for Industry 4.0: Roles, Capabilities, and Applications. *Sens. Int.* **2021**, *2*, 100110. [CrossRef]
32. Naresh, V.; Lee, N. A Review on Biosensors and Recent Development of Nanostructured Materials-Enabled Biosensors. *Sensors* **2021**, *21*, 1109. [CrossRef]
33. Ensafi, A.A. Chapter 1—An Introduction to Sensors and Biosensors. In *Electrochemical Biosensors*; Ensafi, A.A., Ed.; Elsevier: Amsterdam, The Netherlands, 2019; pp. 1–10, ISBN 978-0-12-816491-4.
34. Stikic, M.; Larlus, D.; Ebert, S.; Schiele, B. Weakly Supervised Recognition of Daily Life Activities with Wearable Sensors. *IEEE Trans. Pattern Anal. Mach. Intell.* **2011**, *33*, 2521–2537. [CrossRef] [PubMed]
35. Zhang, S.; Ang, M.H.; Xiao, W.; Tham, C.K. Detection of Activities by Wireless Sensors for Daily Life Surveillance: Eating and Drinking. *Sensors* **2009**, *9*, 1499–1517. [CrossRef] [PubMed]
36. Jia, Y.-H.; Sun, Y.-X.; Gao, L.-L.; Sun, Y.; Deng, Z.-P.; Li, J.-G.; Zhao, B.; Ji, B.-T. A Highly Selective and Sensitive Rhodamine B-Based Chemosensor for Sn^{4+} in Water-Bearing and Biomaging and Biosensing in Zebrafish. *Spectrochim. Acta Part A Mol. Biomol. Spectrosc.* **2024**, *317*, 124385. [CrossRef] [PubMed]
37. Quan, W.; Zhao, W.; Duan, X.; Yan, R.; Chen, Y.; Xu, D. Highly Sensitive Pt-Functionalized In_2O_3/SnS_2 Nanoflowers to Realize the Rapid Detection of H_2S Gas. *Sens. Actuators A Phys.* **2024**, *371*, 115306. [CrossRef]
38. Lee, B.; Cho, S.; Jeong, B.J.; Lee, S.H.; Kim, D.; Kim, S.H.; Park, J.-H.; Yu, H.K.; Choi, J.-Y. Highly Responsive Hydrogen Sensor Based on Pd Nanoparticle-Decorated Transfer-Free 3D Graphene. *Sens. Actuators B Chem.* **2024**, *401*, 134913. [CrossRef]
39. Munusami, V.; Arutselvan, K.; Vadivel, S. Development of High Sensitivity LPG and NO_2 Gas Sensor Based $ZnGa_2O_4$/Graphene Nanoplates Hybrid Structure—A Novel Approach. *Diam. Relat. Mater.* **2021**, *111*, 108167. [CrossRef]
40. Niyitanga, T.; Chaudhary, A.; Ahmad, K.; Kim, H. Titanium Carbide ($Ti_3C_2T_x$) MXene as Efficient Electron/Hole Transport Material for Perovskite Solar Cells and Electrode Material for Electrochemical Biosensors/Non-Biosensors Applications. *Micromachines* **2023**, *14*, 1907. [CrossRef] [PubMed]
41. Shahzad, F.; Alhabeb, M.; Hatter, C.B.; Anasori, B.; Man Hong, S.; Koo, C.M.; Gogotsi, Y. Electromagnetic Interference Shielding with 2D Transition Metal Carbides (MXenes). *Science* **2016**, *353*, 1137–1140. [CrossRef]
42. Mariano, M.; Mashtalir, O.; Antonio, F.Q.; Ryu, W.-H.; Deng, B.; Xia, F.; Gogotsi, Y.; Taylor, A.D. Solution-Processed Titanium Carbide MXene Films Examined as Highly Transparent Conductors. *Nanoscale* **2016**, *8*, 16371–16378. [CrossRef]
43. Liu, L.-X.; Chen, W.; Zhang, H.-B.; Ye, L.; Wang, Z.; Zhang, Y.; Min, P.; Yu, Z.-Z. Super-Tough and Environmentally Stable Aramid. Nanofiber@MXene Coaxial Fibers with Outstanding Electromagnetic Interference Shielding Efficiency. *Nano-Micro Lett.* **2022**, *14*, 111. [CrossRef]
44. Navitski, I.; Ramanaviciute, A.; Ramanavicius, S.; Pogorielov, M.; Ramanavicius, A. MXene-Based Chemo-Sensors and Other Sensing Devices. *Nanomaterials* **2024**, *14*, 447. [CrossRef] [PubMed]
45. Limbu, T.B.; Chitara, B.; Garcia Cervantes, M.Y.; Zhou, Y.; Huang, S.; Tang, Y.; Yan, F. Unravelling the Thickness Dependence and Mechanism of Surface-Enhanced Raman Scattering on $Ti_3C_2T_X$ MXene Nanosheets. *J. Phys. Chem. C* **2020**, *124*, 17772–17782. [CrossRef]
46. Feng, Y.; Zhou, F.; Deng, Q.; Peng, C. Solvothermal Synthesis of in Situ Nitrogen-Doped Ti_3C_2 MXene Fluorescent Quantum Dots for Selective Cu^{2+} Detection. *Ceram. Int.* **2020**, *46*, 8320–8327. [CrossRef]
47. Zhu, X.; Zhang, Y.; Liu, M.; Liu, Y. 2D Titanium Carbide MXenes as Emerging Optical Biosensing Platforms. *Biosens. Bioelectron.* **2021**, *171*, 112730. [CrossRef] [PubMed]
48. Jiang, X.; Kuklin, A.V.; Baev, A.; Ge, Y.; Ågren, H.; Zhang, H.; Prasad, P.N. Two-Dimensional MXenes: From Morphological to Optical, Electric, and Magnetic Properties and Applications. *Phys. Rep.* **2020**, *848*, 1–58. [CrossRef]
49. Wang, Y.; Xu, Y.; Hu, M.; Ling, H.; Zhu, X. MXenes: Focus on Optical and Electronic Properties and Corresponding Applications. *Nanophotonics* **2020**, *9*, 1601–1620. [CrossRef]
50. Wu, L.; Yuan, X.; Tang, Y.; Wageh, S.; Al-Hartomy, O.A.; Al-Sehemi, A.G.; Yang, J.; Xiang, Y.; Zhang, H.; Qin, Y. MXene Sensors Based on Optical and Electrical Sensing Signals: From Biological, Chemical, and Physical Sensing to Emerging Intelligent and Bionic Devices. *PhotoniX* **2023**, *4*, 15. [CrossRef]
51. Nižetić, S.; Šolić, P.; López-de-Ipiña González-de-Artaza, D.; Patrono, L. Internet of Things (IoT): Opportunities, Issues and Challenges towards a Smart and Sustainable Future. *J. Clean. Prod.* **2020**, *274*, 122877. [CrossRef] [PubMed]

52. Shei, R.-J.; Holder, I.G.; Oumsang, A.S.; Paris, B.A.; Paris, H.L. Wearable Activity Trackers–Advanced Technology or Advanced Marketing? *Eur. J. Appl. Physiol.* **2022**, *122*, 1975–1990. [CrossRef]
53. Márquez-Sánchez, S.; Huerta-Muñoz, J.; Herrera-Santos, J.; Arrieta, A.G.; De la Prieta, F. Gas Sensing in Industry. A Case Study: Train Hangar. *Ad Hoc Netw.* **2023**, *148*, 103205. [CrossRef]
54. Fuśnik, Ł.; Szafraniak, B.; Paleczek, A.; Grochala, D.; Rydosz, A. A Review of Gas Measurement Set-ups. *Sensors* **2022**, *22*, 2557. [CrossRef] [PubMed]
55. Yaqoob, U.; Younis, M.I. Chemical Gas Sensors: Recent Developments, Challenges, and the Potential of Machine Learning—A Review. *Sensors* **2021**, *21*, 2877. [CrossRef] [PubMed]
56. Dhall, S.; Mehta, B.R.; Tyagi, A.K.; Sood, K. A Review on Environmental Gas Sensors: Materials and Technologies. *Sens. Int.* **2021**, *2*, 100116. [CrossRef]
57. Umapathi, R.; Park, B.; Sonwal, S.; Rani, G.M.; Cho, Y.; Huh, Y.S. Advances in Optical-Sensing Strategies for the on-Site Detection of Pesticides in Agricultural Foods. *Trends Food Sci. Technol.* **2022**, *119*, 69–89. [CrossRef]
58. Bhardwaj, N.; Bhardwaj, S.K.; Bhatt, D.; Lim, D.K.; Kim, K.-H.; Deep, A. Optical Detection of Waterborne Pathogens Using Nanomaterials. *TrAC Trends Anal. Chem.* **2019**, *113*, 280–300. [CrossRef]
59. Kaushal, J.B.; Raut, P.; Kumar, S. Organic Electronics in Biosensing: A Promising Frontier for Medical and Environmental Applications. *Biosensors* **2023**, *13*, 976. [CrossRef]
60. Long, F.; Zhu, A.; Shi, H. Recent Advances in Optical Biosensors for Environmental Monitoring and Early Warning. *Sensors* **2013**, *13*, 13928–13948. [CrossRef] [PubMed]
61. Maleski, K.; Alhabeb, M. Top-Down MXene Synthesis (Selective Etching). In *2D Metal Carbides and Nitrides (MXenes): Structure, Properties and Applications*; Anasori, B., Gogotsi, Y., Eds.; Springer International Publishing: Cham, Switzerland, 2019; pp. 69–87, ISBN 978-3-030-19026-2.
62. Naguib, M.; Gogotsi, Y. Synthesis of Two-Dimensional Materials by Selective Extraction. *Acc. Chem. Res.* **2015**, *48*, 128–135. [CrossRef]
63. Malaki, M.; Maleki, A.; Varma, R.S. MXenes and Ultrasonication. *J. Mater. Chem. A* **2019**, *7*, 10843–10857. [CrossRef]
64. Mashtalir, O.; Naguib, M.; Dyatkin, B.; Gogotsi, Y.; Barsoum, M.W. Kinetics of Aluminum Extraction from Ti_3AlC_2 in Hydrofluoric Acid. *Mater. Chem. Phys.* **2013**, *139*, 147–152. [CrossRef]
65. Sang, X.; Xie, Y.; Lin, M.-W.; Alhabeb, M.; Van Aken, K.L.; Gogotsi, Y.; Kent, P.R.C.; Xiao, K.; Unocic, R.R. Atomic Defects in Monolayer Titanium Carbide ($Ti_3C_2T_x$) MXene. *ACS Nano* **2016**, *10*, 9193–9200. [CrossRef] [PubMed]
66. Ahmed, A.; Hossain, M.M.; Adak, B.; Mukhopadhyay, S. Recent Advances in 2D MXene Integrated Smart-Textile Interfaces for Multifunctional Applications. *Chem. Mater.* **2020**, *32*, 10296–10320. [CrossRef]
67. Alhabeb, M.; Maleski, K.; Anasori, B.; Lelyukh, P.; Clark, L.; Sin, S.; Gogotsi, Y. Guidelines for Synthesis and Processing of Two-Dimensional Titanium Carbide ($Ti_3C_2T_x$ MXene). *Chem. Mater.* **2017**, *29*, 7633–7644. [CrossRef]
68. Ghidiu, M.; Lukatskaya, M.R.; Zhao, M.-Q.; Gogotsi, Y.; Barsoum, M.W. Conductive Two-Dimensional Titanium Carbide 'Clay' with High Volumetric Capacitance. *Nature* **2014**, *516*, 78–81. [CrossRef] [PubMed]
69. Lipatov, A.; Alhabeb, M.; Lukatskaya, M.R.; Boson, A.; Gogotsi, Y.; Sinitskii, A. Effect of Synthesis on Quality, Electronic Properties and Environmental Stability of Individual Monolayer Ti_3C_2 MXene Flakes. *Adv. Electron. Mater.* **2016**, *2*, 1600255. [CrossRef]
70. Naguib, M.; Mashtalir, O.; Carle, J.; Presser, V.; Lu, J.; Hultman, L.; Gogotsi, Y.; Barsoum, M.W. Two-Dimensional Transition Metal Carbides. *ACS Nano* **2012**, *6*, 1322–1331. [CrossRef] [PubMed]
71. Zhang, C.; Cui, L.; Abdolhosseinzadeh, S.; Heier, J. Two-Dimensional MXenes for Lithium-Sulfur Batteries. *InfoMat* **2020**, *2*, 613–638. [CrossRef]
72. Xu, C.; Wang, L.; Liu, Z.; Chen, L.; Guo, J.; Kang, N.; Ma, X.-L.; Cheng, H.-M.; Ren, W. Large-Area High-Quality 2D Ultrathin Mo_2C Superconducting Crystals. *Nat. Mater.* **2015**, *14*, 1135–1141. [CrossRef]
73. Xu, C.; Chen, L.; Liu, Z.; Cheng, H.-M.; Ren, W. Bottom-Up Synthesis of 2D Transition Metal Carbides and Nitrides. In *2D Metal Carbides and Nitrides (MXenes): Structure, Properties and Applications*; Anasori, B., Gogotsi, Y., Eds.; Springer International Publishing: Cham, Switzerland, 2019; pp. 89–109, ISBN 978-3-030-19026-2.
74. Xiao, X.; Yu, H.; Jin, H.; Wu, M.; Fang, Y.; Sun, J.; Hu, Z.; Li, T.; Wu, J.; Huang, L.; et al. Salt-Templated Synthesis of 2D Metallic MoN and Other Nitrides. *ACS Nano* **2017**, *11*, 2180–2186. [CrossRef]
75. Zhang, Z.; Zhang, F.; Wang, H.; Chan, C.H.; Lu, W.; Dai, J. Substrate Orientation-Induced Epitaxial Growth of Face Centered Cubic Mo_2C Superconductive Thin Film. *J. Mater. Chem. C* **2017**, *5*, 10822–10827. [CrossRef]
76. Ahmad, K.; Khan, M.Q.; Raza, W.; Gondal, M.A. Recent Progress in Metal–Organic Frameworks for the Fabrication of Chemical Sensors. In *Metal–Organic Frameworks for Environmental Sensing*; ACS Symposium Series; American Chemical Society: Washington, DC, USA, 2021; Volume 1394, pp. 71–82, ISBN 978-0-8412-9810-1.
77. Ahmad, K.; Raza, W. Fabrication of Electrochemical Sensors for the Sensing of Hazardous Compounds. In *Handbook of Nanomaterials and Nanocomposites for Energy and Environmental Applications*; Kharissova, O.V., Torres-Martínez, L.M., Kharisov, B.I., Eds.; Springer International Publishing: Cham, Switzerland, 2021; pp. 1799–1816, ISBN 978-3-030-36268-3.
78. Raza, W.; Ahmad, K.; Kim, H. Nitrogen-Doped Graphene as an Efficient Metal-Free Catalyst for Ammonia and Non-Enzymatic Glucose Sensing. *J. Phys. Chem. Solids* **2022**, *160*, 110359. [CrossRef]

79. Raza, W.; Ahmad, K. Room Temperature Gas Sensor Based on Reduce Graphene Oxide for Environmental Monitoring. In *Handbook of Nanomaterials and Nanocomposites for Energy and Environmental Applications*; Kharissova, O.V., Martínez, L.M.T., Kharisov, B.I., Eds.; Springer International Publishing: Cham, Switzerland, 2020; pp. 1–19, ISBN 978-3-030-11155-7.
80. Khan, M.Q.; Ahmad, K.; Raza, W.; Khan, R.A.; Sutradhar, M.; Paul, A. Hydrothermally Synthesized MoS_2 as Electrochemical Catalyst for the Fabrication of Thiabendazole Electrochemical Sensor and Dye Sensitized Solar Cells. *Catalysts* **2024**, *14*, 107. [CrossRef]
81. Ahmad, K.; Raza, W.; Alsulmi, A.; Kim, H. Design and Fabrication of MnO_2 @ZIF-8 Composite for Electrochemical Sensing of Environment Pollutant Hydrogen Peroxide. *Colloids Surf. A Physicochem. Eng. Asp.* **2023**, *674*, 131937. [CrossRef]
82. Ahmad, K.; Raza, W.; Khan, R.A. Ti_3AlC_2 MAX Phase Modified Screen-Printed Electrode for the Fabrication of Hydrazine Sensor. *Micromachines* **2024**, *15*, 633. [CrossRef]
83. Wu, X.; Ma, P.; Sun, Y.; Du, F.; Song, D.; Xu, G. Application of MXene in Electrochemical Sensors: A Review. *Electroanalysis* **2021**, *33*, 1827–1851. [CrossRef]
84. Yang, M.; Lu, H.; Liu, S. Recent Advances of MXene-Based Electrochemical Immunosensors. *Appl. Sci.* **2022**, *12*, 5630. [CrossRef]
85. Tran, V.A.; Tran, N.T.; Doan, V.D.; Nguyen, T.Q.; Thi, H.H.P.; Vo, G.N.L. Application Prospects of MXenes Materials Modifications for Sensors. *Micromachines* **2023**, *14*, 247. [CrossRef]
86. Atkare, S.; Kaushik, S.D.; Jagtap, S.; Rout, C.S. Room-Temperature Chemiresistive Ammonia Sensors Based on 2D MXenes and Their Hybrids: Recent Developments and Future Prospects. *Dalton Trans.* **2023**, *52*, 13831–13851. [CrossRef]
87. Sun, Z.M. Progress in Research and Development on MAX Phases: A Family of Layered Ternary Compounds. *Int. Mater. Rev.* **2011**, *56*, 143–166. [CrossRef]
88. Devaraj, M.; Rajendran, S.; Hoang, T.K.A.; Soto-Moscoso, M. A Review on MXene and Its Nanocomposites for the Detection of Toxic Inorganic Gases. *Chemosphere* **2022**, *302*, 134933. [CrossRef]
89. Wu, M.; He, M.; Hu, Q.; Wu, Q.; Sun, G.; Xie, L.; Zhang, Z.; Zhu, Z.; Zhou, A. Ti_3C_2 MXene-Based Sensors with High Selectivity for NH_3 Detection at Room Temperature. *ACS Sens.* **2019**, *4*, 2763–2770. [CrossRef] [PubMed]
90. Wang, S.; Jiang, Y.; Liu, B.; Duan, Z.; Pan, H.; Yuan, Z.; Xie, G.; Wang, J.; Fang, Z.; Tai, H. Ultrathin Nb_2CT_x Nanosheets-Supported Polyaniline Nanocomposite: Enabling Ultrasensitive NH_3 Detection. *Sens. Actuators B Chem.* **2021**, *343*, 130069. [CrossRef]
91. Thomas, T.; Ramos Ramón, J.A.; Agarwal, V.; Méndez, A.Á.; Martinez, J.A.A.; Kumar, Y.; Sanal, K.C. Highly Stable, Fast Responsive Mo_2CT_x MXene Sensors for Room Temperature Carbon Dioxide Detection. *Microporous Mesoporous Mater.* **2022**, *336*, 111872. [CrossRef]
92. Sun, B.; Lv, H.; Liu, Z.; Wang, J.; Bai, X.; Zhang, Y.; Chen, J.; Kan, K.; Shi, K. Co_3O_4@PEI/$Ti_3C_2T_x$ MXene Nanocomposites for a Highly Sensitive NO_x Gas Sensor with a Low Detection Limit. *J. Mater. Chem. A* **2021**, *9*, 6335–6344. [CrossRef]
93. Lee, S.H.; Eom, W.; Shin, H.; Ambade, R.B.; Bang, J.H.; Kim, H.W.; Han, T.H. Room-Temperature, Highly Durable $Ti_3C_2T_x$ MXene/Graphene Hybrid Fibers for NH_3 Gas Sensing. *ACS Appl. Mater. Interfaces* **2020**, *12*, 10434–10442. [CrossRef] [PubMed]
94. Yu, X.F.; Li, Y.C.; Cheng, J.B.; Liu, Z.B.; Li, Q.Z.; Li, W.Z.; Yang, X.; Xiao, B. Monolayer Ti_2CO_2: A Promising Candidate for NH_3 Sensor or Capturer with High Sensitivity and Selectivity. *ACS Appl. Mater. Interfaces* **2015**, *7*, 13707–13713. [CrossRef]
95. Xiao, B.; Li, Y.; Yu, X.; Cheng, J. MXenes: Reusable Materials for NH_3 Sensor or Capturer by Controlling the Charge Injection. *Sens. Actuators B Chem.* **2016**, *235*, 103–109. [CrossRef]
96. Ma, S.; Yuan, D.; Jiao, Z.; Wang, T.; Dai, X. Monolayer Sc_2CO_2: A Promising Candidate as a SO_2 Gas Sensor or Capturer. *J. Phys. Chem. C* **2017**, *121*, 24077–24084. [CrossRef]
97. Yang, D.; Fan, X.; Zhao, D.; An, Y.; Hu, Y.; Luo, Z. Sc_2CO_2 and Mn-Doped Sc_2CO_2 as Gas Sensor Materials to NO and CO: A First-Principles Study. *Phys. E Low-Dimens. Syst. Nanostruct.* **2019**, *111*, 84–90. [CrossRef]
98. Lee, E.; Vahidmohammadi, A.; Prorok, B.C.; Yoon, Y.S.; Beidaghi, M.; Kim, D.J. Room Temperature Gas Sensing of Two-Dimensional Titanium Carbide (MXene). *ACS Appl. Mater. Interfaces* **2017**, *9*, 37184–37190. [CrossRef]
99. Kim, S.J.; Koh, H.J.; Ren, C.E.; Kwon, O.; Maleski, K.; Cho, S.Y.; Anasori, B.; Kim, C.K.; Choi, Y.K.; Kim, J.; et al. Metallic $Ti_3C_2T_x$ MXene Gas Sensors with Ultrahigh Signal-to-Noise Ratio. *ACS Nano* **2018**, *12*, 986–993. [CrossRef] [PubMed]
100. Shuck, C.E.; Han, M.; Maleski, K.; Hantanasirisakul, K.; Kim, S.J.; Choi, J.; Reil, W.E.B.; Gogotsi, Y. Effect of Ti_3AlC_2 MAX Phase on Structure and Properties of Resultant $Ti_3C_2T_x$ MXene. *ACS Appl. Nano Mater.* **2019**, *2*, 3368–3376. [CrossRef]
101. Zhao, Q.; Sun, D.; Wang, S.; Duan, Z.; Yuan, Z.; Wei, G.; Xu, J.-L.; Tai, H.; Jiang, Y. Enhanced Blocking Effect: A New Strategy to Improve the NO_2 Sensing Performance of $Ti_3C_2T_x$ by γ-Poly(l-Glutamic Acid) Modification. *ACS Sens.* **2021**, *6*, 2858–2867. [CrossRef]
102. Zhang, Y.; Jiang, Y.; Duan, Z.; Huang, Q.; Wu, Y.; Liu, B.; Zhao, Q.; Wang, S.; Yuan, Z.; Tai, H. Highly Sensitive and Selective NO_2 Sensor of Alkalized V_2CT_x MXene Driven by Interlayer Swelling. *Sens. Actuators B Chem.* **2021**, *344*, 130150. [CrossRef]
103. Chae, Y.; Kim, S.J.; Cho, S.-Y.; Choi, J.; Maleski, K.; Lee, B.-J.; Jung, H.-T.; Gogotsi, Y.; Lee, Y.; Ahn, C.W. An Investigation into the Factors Governing the Oxidation of Two-Dimensional Ti_3C_2 MXene. *Nanoscale* **2019**, *11*, 8387–8393. [CrossRef]
104. Yuan, W.; Yang, K.; Peng, H.; Li, F.; Yin, F. A Flexible VOCs Sensor Based on a 3D Mxene Framework with a High Sensing Performance. *J. Mater. Chem. A* **2018**, *6*, 18116–18124. [CrossRef]
105. Yang, Z.; Liu, A.; Wang, C.; Liu, F.; He, J.; Li, S.; Wang, J.; You, R.; Yan, X.; Sun, P.; et al. Improvement of Gas and Humidity Sensing Properties of Organ-like MXene by Alkaline Treatment. *ACS Sens.* **2019**, *4*, 1261–1269. [CrossRef]

106. Koh, H.-J.; Kim, S.J.; Maleski, K.; Cho, S.-Y.; Kim, Y.-J.; Ahn, C.W.; Gogotsi, Y.; Jung, H.-T. Enhanced Selectivity of MXene Gas Sensors through Metal Ion Intercalation: In Situ X-Ray Diffraction Study. *ACS Sens.* **2019**, *4*, 1365–1372. [CrossRef] [PubMed]
107. Lee, E.; VahidMohammadi, A.; Yoon, Y.S.; Beidaghi, M.; Kim, D.-J. Two-Dimensional Vanadium Carbide MXene for Gas Sensors with Ultrahigh Sensitivity Toward Nonpolar Gases. *ACS Sens.* **2019**, *4*, 1603–1611. [CrossRef]
108. Zhao, W.-N.; Yun, N.; Dai, Z.-H.; Li, Y.-F. A High-Performance Trace Level Acetone Sensor Using an Indispensable $V_4C_3T_x$ MXene. *RSC Adv.* **2020**, *10*, 1261–1270. [CrossRef]
109. Guo, W.; Surya, S.G.; Babar, V.; Ming, F.; Sharma, S.; Alshareef, H.N.; Schwingenschlögl, U.; Salama, K.N. Selective Toluene Detection with Mo_2CT_x MXene at Room Temperature. *ACS Appl. Mater. Interfaces* **2020**, *12*, 57218–57227. [CrossRef] [PubMed]
110. Cho, S.-Y.; Kim, J.Y.; Kwon, O.; Kim, J.; Jung, H.-T. Molybdenum Carbide Chemical Sensors with Ultrahigh Signal-to-Noise Ratios and Ambient Stability. *J. Mater. Chem. A* **2018**, *6*, 23408–23416. [CrossRef]
111. Tai, H.; Duan, Z.; He, Z.; Li, X.; Xu, J.; Liu, B.; Jiang, Y. Enhanced Ammonia Response of $Ti_3C_2T_x$ Nanosheets Supported by TiO_2 Nanoparticles at Room Temperature. *Sens. Actuators B Chem.* **2019**, *298*, 126874. [CrossRef]
112. He, T.; Liu, W.; Lv, T.; Ma, M.; Liu, Z.; Vasiliev, A.; Li, X. MXene/SnO_2 Heterojunction Based Chemical Gas Sensors. *Sens. Actuators B Chem.* **2021**, *329*, 129275. [CrossRef]
113. Wang, D.; Zhang, D.; Guo, J.; Hu, Y.; Yang, Y.; Sun, T.; Zhang, H.; Liu, X. Multifunctional Poly(Vinyl Alcohol)/Ag Nanofibers-Based Triboelectric Nanogenerator for Self-Powered MXene/Tungsten Oxide Nanohybrid NO_2 Gas Sensor. *Nano Energy* **2021**, *89*, 106410. [CrossRef]
114. Chen, T.; Yan, W.; Wang, Y.; Li, J.; Hu, H.; Ho, D. SnS_2/MXene Derived TiO_2 Hybrid for Ultra-Fast Room Temperature NO_2 Gas Sensing. *J. Mater. Chem. C* **2021**, *9*, 7407–7416. [CrossRef]
115. Xia, Y.; He, S.; Wang, J.; Zhou, L.; Wang, J.; Komarneni, S. MXene/WS2 Hybrids for Visible-Light-Activated NO_2 Sensing at Room Temperature. *Chem. Commun.* **2021**, *57*, 9136–9139. [CrossRef] [PubMed]
116. Zhao, Q.; Zhou, W.; Zhang, M.; Wang, Y.; Duan, Z.; Tan, C.; Liu, B.; Ouyang, F.; Yuan, Z.; Tai, H.; et al. Edge-Enriched $Mo_2TiC_2T_x/MoS_2$ Heterostructure with Coupling Interface for Selective NO_2 Monitoring. *Adv. Funct. Mater.* **2022**, *32*, 2203528. [CrossRef]
117. Zhang, Y.; Li, Y.; Jiang, Y.; Duan, Z.; Yuan, Z.; Liu, B.; Huang, Q.; Zhao, Q.; Yang, Y.; Tai, H. Synergistic Effect of Charge Transfer and Interlayer Swelling in V_2CT_x/SnS_2 Driving Ultrafast and Highly Sensitive NO_2 Detection at Room Temperature. *Sens. Actuators B Chem.* **2024**, *411*, 135788. [CrossRef]
118. Hou, M.; Gao, J.; Yang, L.; Guo, S.; Hu, T.; Li, Y. Room Temperature Gas Sensing under UV Light Irradiation for $Ti_3C_2T_x$ MXene Derived Lamellar TiO_2-C/g-C_3N_4 Composites. *Appl. Surf. Sci.* **2021**, *535*, 147666. [CrossRef]
119. Li, X.; Xu, J.; Jiang, Y.; He, Z.; Liu, B.; Xie, H.; Li, H.; Li, Z.; Wang, Y.; Tai, H. Toward Agricultural Ammonia Volatilization Monitoring: A Flexible Polyaniline/$Ti_3C_2T_x$ Hybrid Sensitive Films Based Gas Sensor. *Sens. Actuators B Chem.* **2020**, *316*, 128144. [CrossRef]
120. Chen, P.; Zhao, Z.; Shao, Z.; Tian, Y.; Li, B.; Huang, B.; Zhang, S.; Liu, C.; Shen, X. Highly Selective NH_3 Gas Sensor Based on Polypyrrole/$Ti_3C_2T_x$ Nanocomposites Operating at Room Temperature. *J. Mater. Sci. Mater. Electron.* **2022**, *33*, 6168–6177. [CrossRef]
121. Jin, L.; Wu, C.; Wei, K.; He, L.; Gao, H.; Zhang, H.; Zhang, K.; Asiri, A.M.; Alamry, K.A.; Yang, L.; et al. Polymeric $Ti_3C_2T_x$ MXene Composites for Room Temperature Ammonia Sensing. *ACS Appl. Nano Mater.* **2020**, *3*, 12071–12079. [CrossRef]
122. Zhou, Y.; Wang, Y.; Wang, Y.; Li, X. Humidity-Enabled Ionic Conductive Trace Carbon Dioxide Sensing of Nitrogen-Doped $Ti_3C_2T_x$ MXene/Polyethyleneimine Composite Films Decorated with Reduced Graphene Oxide Nanosheets. *Anal. Chem.* **2020**, *92*, 16033–16042. [CrossRef] [PubMed]
123. Sun, Q.; Wang, J.; Wang, X.; Dai, J.; Wang, X.; Fan, H.; Wang, Z.; Li, H.; Huang, X.; Huang, W. Treatment-Dependent Surface Chemistry and Gas Sensing Behavior of the Thinnest Member of Titanium Carbide MXenes. *Nanoscale* **2020**, *12*, 16987–16994. [CrossRef] [PubMed]
124. Hermawan, A.; Zhang, B.; Taufik, A.; Asakura, Y.; Hasegawa, T.; Zhu, J.; Shi, P.; Yin, S. CuO Nanoparticles/$Ti_3C_2T_x$ MXene Hybrid Nanocomposites for Detection of Toluene Gas. *ACS Appl. Nano Mater.* **2020**, *3*, 4755–4766. [CrossRef]
125. Chen, W.Y.; Jiang, X.; Lai, S.-N.; Peroulis, D.; Stanciu, L. Nanohybrids of a MXene and Transition Metal Dichalcogenide for Selective Detection of Volatile Organic Compounds. *Nat. Commun.* **2020**, *11*, 1302. [CrossRef]
126. Yang, Z.; Jiang, L.; Wang, J.; Liu, F.; He, J.; Liu, A.; Lv, S.; You, R.; Yan, X.; Sun, P.; et al. Flexible Resistive NO_2 Gas Sensor of Three-Dimensional Crumpled MXene $Ti_3C_2T_x$/ZnO Spheres for Room Temperature Application. *Sens. Actuators B Chem.* **2021**, *326*, 128828. [CrossRef]
127. Sima, Z.; Song, P.; Ding, Y.; Lu, Z.; Wang, Q. $ZnSnO_3$ Nanocubes/$Ti_3C_2T_x$ MXene Composites for Enhanced Formaldehyde Gas Sensing Properties at Room Temperature. *Appl. Surf. Sci.* **2022**, *598*, 153861. [CrossRef]
128. Liu, M.; Wang, Z.; Song, P.; Yang, Z.; Wang, Q. In_2O_3 Nanocubes/$Ti_3C_2T_x$ MXene Composites for Enhanced Methanol Gas Sensing Properties at Room Temperature. *Ceram. Int.* **2021**, *47*, 23028–23037. [CrossRef]
129. Liu, M.; Ji, J.; Song, P.; Liu, M.; Wang, Q. α-Fe_2O_3 Nanocubes/$Ti_3C_2T_x$ MXene Composites for Improvement of Acetone Sensing Performance at Room Temperature. *Sens. Actuators B Chem.* **2021**, *349*, 130782. [CrossRef]
130. Wang, S.; Liu, B.; Duan, Z.; Zhao, Q.; Zhang, Y.; Xie, G.; Jiang, Y.; Li, S.; Tai, H. PANI Nanofibers-Supported Nb_2CT_x Nanosheets-Enabled Selective NH_3 Detection Driven by TENG at Room Temperature. *Sens. Actuators B Chem.* **2021**, *327*, 128923. [CrossRef]

131. Lashgari, H.; Abolhassani, M.R.; Boochani, A.; Elahi, S.M.; Khodadadi, J. Electronic and Optical Properties of 2D Graphene-like Compounds Titanium Carbides and Nitrides: DFT Calculations. *Solid State Commun.* **2014**, *195*, 61–69. [CrossRef]
132. Zhang, H.; Yang, G.; Zuo, X.; Tang, H.; Yang, Q.; Li, G. Computational Studies on the Structural, Electronic and Optical Properties of Graphene-like MXenes (M2CT2, M = Ti, Zr, Hf; T = O, F, OH) and Their Potential Applications as Visible-Light Driven Photocatalysts. *J. Mater. Chem. A* **2016**, *4*, 12913–12920. [CrossRef]
133. Halim, J.; Lukatskaya, M.R.; Cook, K.M.; Lu, J.; Smith, C.R.; Näslund, L.-Å.; May, S.J.; Hultman, L.; Gogotsi, Y.; Eklund, P.; et al. Transparent Conductive Two-Dimensional Titanium Carbide Epitaxial Thin Films. *Chem. Mater.* **2014**, *26*, 2374–2381. [CrossRef] [PubMed]
134. Maleski, K.; Ren, C.E.; Zhao, M.-Q.; Anasori, B.; Gogotsi, Y. Size-Dependent Physical and Electrochemical Properties of Two-Dimensional MXene Flakes. *ACS Appl. Mater. Interfaces* **2018**, *10*, 24491–24498. [CrossRef] [PubMed]
135. Zang, X.; Wang, J.; Qin, Y.; Wang, T.; He, C.; Shao, Q.; Zhu, H.; Cao, N. Enhancing Capacitance Performance of $Ti_3C_2T_x$ MXene as Electrode Materials of Supercapacitor: From Controlled Preparation to Composite Structure Construction. *Nano-Micro Lett.* **2020**, *12*, 77. [CrossRef] [PubMed]
136. Deshmukh, K.; Kovářík, T.; Khadheer Pasha, S.K. State of the Art Recent Progress in Two Dimensional MXenes Based Gas Sensors and Biosensors: A Comprehensive Review. *Coord. Chem. Rev.* **2020**, *424*, 213514. [CrossRef]
137. Berdiyorov, G.R.; Mahmoud, K.A. Effect of Surface Termination on Ion Intercalation Selectivity of Bilayer Ti3C2T2 (T = F, O and OH) MXene. *Appl. Surf. Sci.* **2017**, *416*, 725–730. [CrossRef]
138. Bai, Y.; Zhou, K.; Srikanth, N.; Pang, J.H.L.; He, X.; Wang, R. Dependence of Elastic and Optical Properties on Surface Terminated Groups in Two-Dimensional MXene Monolayers: A First-Principles Study. *RSC Adv.* **2016**, *6*, 35731–35739. [CrossRef]
139. Wang, Y.; Wang, S.; Dong, N.; Kang, W.; Li, K.; Nie, Z. Titanium Carbide MXenes Mediated In Situ Reduction Allows Label-Free and Visualized Nanoplasmonic Sensing of Silver Ions. *Anal. Chem.* **2020**, *92*, 4623–4629. [CrossRef] [PubMed]
140. Li, Y.; Kang, Z.; Kong, L.; Shi, H.; Zhang, Y.; Cui, M.; Yang, D.-P. MXene-Ti_3C_2/CuS Nanocomposites: Enhanced Peroxidase-like Activity and Sensitive Colorimetric Cholesterol Detection. *Mater. Sci. Eng. C* **2019**, *104*, 110000. [CrossRef] [PubMed]
141. Li, H.; Wen, Y.; Zhu, X.; Wang, J.; Zhang, L.; Sun, B. Novel Heterostructure of a MXene@NiFe-LDH Nanohybrid with Superior Peroxidase-Like Activity for Sensitive Colorimetric Detection of Glutathione. *ACS Sustain. Chem. Eng.* **2020**, *8*, 520–526. [CrossRef]
142. He, Y.; Zhou, X.; Zhou, L.; Zhang, X.; Ma, L.; Jiang, Y.; Gao, J. Self-Reducing Prussian Blue on $Ti_3C_2T_x$ MXene Nanosheets as a Dual-Functional Nanohybrid for Hydrogen Peroxide and Pesticide Sensing. *Ind. Eng. Chem. Res.* **2020**, *59*, 15556–15564. [CrossRef]
143. Li, M.; Peng, X.; Han, Y.; Fan, L.; Liu, Z.; Guo, Y. Ti_3C_2 MXenes with Intrinsic Peroxidase-like Activity for Label-Free and Colorimetric Sensing of Proteins. *Microchem. J.* **2021**, *166*, 106238. [CrossRef]
144. Yesudasu, V.; Pradhan, H.S.; Pandya, R.J. Recent Progress in Surface Plasmon Resonance Based Sensors: A Comprehensive Review. *Heliyon* **2021**, *7*, e06321. [CrossRef] [PubMed]
145. Xu, Y.; Ang, Y.S.; Wu, L.; Ang, L.K. High Sensitivity Surface Plasmon Resonance Sensor Based on Two-Dimensional MXene and Transition Metal Dichalcogenide: A Theoretical Study. *Nanomaterials* **2019**, *9*, 165. [CrossRef]
146. Srivastava, A.; Verma, A.; Das, R.; Prajapati, Y.K. A Theoretical Approach to Improve the Performance of SPR Biosensor Using MXene and Black Phosphorus. *Optik* **2020**, *203*, 163430. [CrossRef]
147. Sudheer, V.R.; Kumar, S.R.S.; Sankararaman, S. Ultrahigh Sensitivity Surface Plasmon Resonance–Based Fiber-Optic Sensors Using Metal-Graphene Layers with $Ti_3C_2T_x$ MXene Overlayers. *Plasmonics* **2020**, *15*, 457–466. [CrossRef]
148. Pandey, A.K. Plasmonic Sensor Utilizing $Ti_3C_2T_x$ MXene Layer and Fluoride Glass Substrate for Bio- and Gas-Sensing Applications: Performance Evaluation. *Photon. Nanostruct.-Fundam. Appl.* **2020**, *42*, 100863. [CrossRef]
149. Wu, Q.; Li, N.; Wang, Y.; Liu, Y.; Xu, Y.; Wei, S.; Wu, J.; Jia, G.; Fang, X.; Chen, F.; et al. A 2D Transition Metal Carbide MXene-Based SPR Biosensor for Ultrasensitive Carcinoembryonic Antigen Detection. *Biosens. Bioelectron.* **2019**, *144*, 111697. [CrossRef] [PubMed]
150. Wu, Q.; Li, N.; Wang, Y.; Xu, Y.; Wu, J.; Jia, G.; Ji, F.; Fang, X.; Chen, F.; Cui, X. Ultrasensitive and Selective Determination of Carcinoembryonic Antigen Using Multifunctional Ultrathin Amino-Functionalized Ti_3C_2-MXene Nanosheets. *Anal. Chem.* **2020**, *92*, 3354–3360. [CrossRef] [PubMed]
151. Wang, P.; Sun, Y.; Li, X.; Wang, L.; Xu, Y.; He, L.; Li, G. Recent Advances in Dual Recognition Based Surface Enhanced Raman Scattering for Pathogenic Bacteria Detection: A Review. *Anal. Chim. Acta* **2021**, *1157*, 338279. [CrossRef] [PubMed]
152. Satheeshkumar, E.; Makaryan, T.; Melikyan, A.; Minassian, H.; Gogotsi, Y.; Yoshimura, M. One-Step Solution Processing of Ag, Au and Pd@MXene Hybrids for SERS. *Sci. Rep.* **2016**, *6*, 32049. [CrossRef] [PubMed]
153. Sarycheva, A.; Makaryan, T.; Maleski, K.; Satheeshkumar, E.; Melikyan, A.; Minassian, H.; Yoshimura, M.; Gogotsi, Y. Two-Dimensional Titanium Carbide (MXene) as Surface-Enhanced Raman Scattering Substrate. *J. Phys. Chem. C* **2017**, *121*, 19983–19988. [CrossRef]
154. Soundiraraju, B.; George, B.K. Two-Dimensional Titanium Nitride (Ti_2N) MXene: Synthesis, Characterization, and Potential Application as Surface-Enhanced Raman Scattering Substrate. *ACS Nano* **2017**, *11*, 8892–8900. [CrossRef] [PubMed]
155. Elumalai, S.; Lombardi, J.R.; Yoshimura, M. The Surface-Enhanced Resonance Raman Scattering of Dye Molecules Adsorbed on Two-Dimensional Titanium Carbide $Ti_3C_2T_x$ (MXene) Film. *Mater. Adv.* **2020**, *1*, 146–152. [CrossRef]

156. Zheng, F.; Ke, W.; Shi, L.; Liu, H.; Zhao, Y. Plasmonic Au–Ag Janus Nanoparticle Engineered Ratiometric Surface-Enhanced Raman Scattering Aptasensor for Ochratoxin A Detection. *Anal. Chem.* **2019**, *91*, 11812–11820. [CrossRef]
157. Medetalibeyoglu, H.; Kotan, G.; Atar, N.; Yola, M.L. A Novel Sandwich-Type SERS Immunosensor for Selective and Sensitive Carcinoembryonic Antigen (CEA) Detection. *Anal. Chim. Acta* **2020**, *1139*, 100–110. [CrossRef]

Disclaimer/Publisher's Note: The statements, opinions and data contained in all publications are solely those of the individual author(s) and contributor(s) and not of MDPI and/or the editor(s). MDPI and/or the editor(s) disclaim responsibility for any injury to people or property resulting from any ideas, methods, instructions or products referred to in the content.